PERFORMANCE ANALYSIS OF GRAPHENE OXIDE CONTACTED PEROVSKITE SOLAR CELL USING SCAPS-1D

MOHAMAD ALIF IKHWAN BIN MD SA’DON

UNIVERSITI TEKNIKAL MALAYSIA MELAKA

PERFORMANCE ANALYSIS OF GRAPHENE OXIDE CONTACTED PEROVSKITE SOLAR CELL USING SCAPS-1D

MOHAMAD ALIF IKHWAN BIN MD SA'DON

This report is submitted in partial fulfilment of the requirements for the degree of Bachelor of Computer Engineering with Honours

Faculty of Electronics and Computer Technology and Engineering
Universiti Teknikal Malaysia Melaka

2024

UNIVERSITI TEKNIKAL MALAYSIA MELAKA
FAKULTI TEKNONOGI KEJUTERAAN ELEKTRONIK DAN KEJURUTERAAN KOMPUTER
BORANG PENGESAHAN STATUS LAPORAN
PROJEK SARJANA MUDA II

Tajuk Projek : MOHAMAD ALIF IKHWAN BIN MD SA'DON
Sesi Pengajian : 2024

Saya MOHAMAD ALIF IKHWAN BIN MD SA'DON mengaku membenarkan laporan Projek Sarjana Muda ini disimpan di Perpustakaan dengan syarat-syarat kegunaan seperti berikut:

1. Laporan adalah hakmilik Universiti Teknikal Malaysia Melaka.
2. Perpustakaan dibenarkan membuat salinan untuk tujuan pengajian sahaja.
3. Perpustakaan dibenarkan membuat salinan laporan ini sebagai bahan pertukaran antara institusi pengajian tinggi.
4. Sila tandakan (✓):

☐	**SULIT***	(Mengandungi maklumat yang berdarjah keselamatan atau kepentingan Malaysia seperti yang termaktub di dalam AKTA RAHSIA RASMI 1972)
☐	**TERHAD***	(Mengandungi maklumat terhad yang telah ditentukan oleh organisasi/badan di mana penyelidikan dijalankan.
/	**TIDAK TERHAD**	

Disahkan oleh:

Profesor Madya Dr. Fauziyah Salehuddin
Profesor Madya
Fakulti Kejuruteraan Elektronik & Kejuruteraan Komputer
Universiti Teknikal Malaysia Melaka
Hang Tuah Jaya, 76100 Durian Tunggal, Melaka

Alamat Tetap: NO 52, JALAN EMAS 4,
TAMAN TENANG JAYA,
85300 SEGAMAT,
JOHOR

Tarikh : 21/1/2024

Tarikh : 23 January 2024

*CATATAN: Jika laporan ini SULIT atau TERHAD, sila lampirkan surat daripada pihak berkuasa/organisasi berkenaan dengan menyatakan sekali tempoh laporan ini perlu dikelaskan sebagai SULIT atau TERHAD.

DECLARATION

I declare that this report entitled "Performance Analysis of Graphene Oxide Contacted Perovskite Solar Cell using SCAPS-1D" is the result of my own work except for quotes as cited in the references.

Signature : ....

Author : MOHAMAD ALIF IKHWAN BIN.SA'DON

Date : 21/1/2024

APPROVAL

I hereby declare that I have read this thesis and in my opinion this thesis is sufficient in terms of scope and quality for the award of Bachelor of Computer Engineering with Honours.

Signature : ....

Supervisor Name : Prof. Madya Ir. Dr. Fauziyah Salehuddin

Date : 23 January 2024

DEDICATION

First and foremost, I am very grateful to all the family members for their valuable guidance and support in the completion of this project in its entirety. I would like to express our deepest appreciation to all those who provided us the possibility to complete our Integrated Design Project. A special gratitude I give to my supervisor, PM. Ir. Dr. Fauziyah Binti Salehuddin whose contribution in stimulating suggestions and encouragement and help me a lot in this project and with much appreciation too because she gave the knowledge about this project to use all required equipment and the necessary materials to complete the project. Besides, not to forget our coordinator of this PSM Project, Dr. Mas Haslinda Binti Mohamad who keep reminding us about the important things that must be implemented before the due date and always give us moral support to complete our project. Next, I also appreciate the guidance given by panels that have improved our project and the knowledge that gives us the idea to complete this project. Finally, gratitude goes to all my friends who directly or indirectly helped me to complete this project.

ABSTRACT

This project studies optimization of graphene oxide (GO) as electron transport layer (ETL) in perovskite solar cells (PSC) using Taguchi method. This method is used to optimize the data from numerical modelling which is Solar Cell Capacitance Simulator-One Dimensional (SCAPS-1D). Taguchi method was reported can find the most prominent factor and reduce variations parameters. The Taguchi algorithm is implemented in this experiment because it is based on orthogonal array (OA) experiments, which provides substantially lower variance for the experiment with optimal control parameter values. SCAPS-1D are used to simulate the PSC with GO as ETL. The simulation results showed that GO as ETL in PSC has produced an efficiency 19.65% using SCAPS-1D simulation. After optimization using Taguchi Method L9 OA the efficiency increased to 25.06 %. This shows that the optimum solution in achieving the desired efficiency in PSC devices was successfully predicted by using Taguchi Method. Overall, the project was a success. The efficiency can be improved by using GO as ETL in PSC devices and optimizing it using Taguchi Method.

ABSTRAK

Projek ini mengkaji pengoptimuman graphene oxide (GO) sebagai lapisan pengangkutan elektron (ETL) dalam sel solar perovskite (PSC) menggunakan kaedah Taguchi. Kaedah ini digunakan untuk mengoptimumkan data daripada pemodelan berangka iaitu Solar Cell Capacitance Simulator- One Dimensional (SCAPS-1D). Kaedah Taguchi dilaporkan boleh mencari faktor yang paling menonjol dan mengurangkan parameter variasi. Algoritma Taguchi dilaksanakan dalam eksperimen ini kerana ia berdasarkan eksperimen tatasusunan ortogon (OA), yang memberikan varians yang jauh lebih rendah untuk eksperimen dengan nilai parameter kawalan optimum. SCAPS-1D digunakan untuk mensimulasikan PSC dengan GO sebagai ETL. Keputusan simulasi menunjukkan bahawa GO sebagai ETL dalam PSC telah menghasilkan kecekapan 19.65% menggunakan simulasi SCAPS-1D. Selepas pengoptimuman menggunakan Kaedah Taguchi L9 OA kecekapan meningkat kepada 25.06%. Ini menunjukkan bahawa penyelesaian optimum dalam mencapai kecekapan yang diingini dalam peranti PSC telah berjaya diramalkan dengan menggunakan Kaedah Taguchi. Secara keseluruhannya, projek itu berjaya. Kecekapan boleh dipertingkatkan dengan menggunakan GO sebagai ETL dalam peranti PSC dan mengoptimumkannya menggunakan Kaedah Taguchi.

ACKNOWLEDGEMENTS

First and foremost, all praises be to Allah S.W.T the most Gracious, the most Merciful, for His showers of blessings giving us strength and patience in this study. Throughout the completion of this project, I would like to express my utmost gratitude toward my project supervisor, PM Ir. Dr. Fauziyah Binti Salehuddin for the germinal ideas, encouragement, guidance, and time throughout the progress of this project. Without her continued support and interest, I could not be able to complete my project successfully. I would like also to thank the Ministry of Higher Education (MOHE) for sponsoring this work under project (FRGS/1/2022/TK07/UTEM/02/47) for the moral support throughout the project and Dr. Marc Burgelman of the University of Gent in Belgium for supplying the SCAPS 1D simulation program.

My deepest gratitude goes to all my family members. All the support that they give to me is the reason where I am now. Without them, I will be lost by myself. Last but not least, I want to extend my sincere thanks to my beloved friends, Shahzan Azfan and Amirul Fitri for being wonderful friends and always there for me through ups and down.

TABLE OF CONTENTS

LIST OF FIGURES

LIST OF TABLES

LIST OF SYMBOLS AND ABBREVIATIONS

For examples:

GO	:	Graphene Oxide
TiO2	:	Titanium Dioxide
Zn	:	Zink Oxide
rGO	:	Reduce Graphene Oxide
ETL	:	Electron Transport Layer
HTL	:	Hole Transport Layer
PSC	:	Perovskite Solar Cell
SCAPS	:	Solar Cell Capacitance Simulator
Jsc	:	Density of Short Circuit Current
Voc	:	Open Circuit Voltage
FF	:	Fill Factor
PCE	:	Power Conversion Efficiency
S/N	:	Signal to noise

CHAPTER 1

INTRODUCTION

This chapter describes the idea of the GO as an ETL layer in the solar cell which includes the background of the project, problem statement, objectives, and scope of the project.

1.1 Background

As we know, solar energy is a potential alternate source of energy in view of the declining fossil fuels. Basically, solar energy is a promising alternative source of energy that harnesses the power of the sun to generate electricity. It is considered one of the cleanest and most abundant renewable energy sources available. Global warming caused by the high emission of carbon dioxide and the effects of greenhouse gases is one of the main concerns of humans today [1]. Carbon oxide in the atmosphere traps the heat reflected from the earth's surface into the atmosphere as a strong aura and as a result makes the earth warmer. In the past decades, continuous efforts have been made in the field of geology and carbon dioxide capture. However, efforts in this field require spending more energy [2,3]. Through research and reports, it has been determined that by 2050, the global energy demand will double with the rapid growth of population and the industrialization of countries, especially in developing countries. Hence, the development of renewable energies without the use of fossil fuels such as thermal wind solar cells, biomass, and hydro-electricity is widely have been studied at global levels. Solar energy is considered a clean energy source. However, the manufacturing cost, size, stability, reproducibility, and high-power conversion efficiency of solar cells are considered an effective approach to improving solar cells. Therefore, there are many researches of solar energy especially in term of power solar cells, such as perovskite solar cells (PSCs), Monocrystalline Silicon Solar Cells, Polycrystalline Silicon Solar Cells, Copper Indium Gallium Selenide Solar cell (CIGS), Organic Solar Cells, Dye-Sensitized Solar Cells (DSSC) and more else. In this paper, perovskite solar cells (PSCs) has been focused in terms on power conversion efficiency (PCE) and sustainability [4].

A solar cell or photovoltaic cell is a solid-state electronic component. which converts a percentage of sunlight energy directly into electricity by the photovoltaic effect, which is a physical and chemical phenomenon. In the past years, various types of solar cells with different functions and structures have been designed and manufactured. The name perovskite is derived from the mineral structure $CaTiO3$, which was discovered by a German mineralogist named Gustav Rose in 1839. It was proposed in 1792-1856 and he chose the name perovskite for this material, which was often considered a promising material for future generations of solar cells the first halogen-based perovskite structure in cesium halide ($CsPbX3$) was observed by

Moller in 1958, and the conductivity characteristics were adjusted and changed by changing the halogen components to achieve different spectral responses. The first appearance of organic cation in halogenated perovskite was proposed and developed for I, CL, and Br by Messrs [5]. Weber and Naturforsch in 1978 Perovskite in photovoltaics began its work in 2001 when Miyasaka and his colleagues used CH3NH3PbBr3 as a sensitizer. began to be applied on TiO_2 for dye-sensitized solar cells, which reached a power conversion efficiency of 2.2% [6].

Nowadays, research on the utilization of perovskite solar cells (PSCs) has gained widespread attention, leading to numerous studies aimed at enhancing both the power conversion efficiency (PCE) and sustainability of this solar cell type. [7]. Introduced in 2009, perovskite solar cells (PSCs) represent a novel class of solar cells that has witnessed remarkable advancements in recent years. A recent research study indicates a notable increase in the power conversion efficiency (PCE) of PSCs, rising from 3.8% to 25.2%, accompanied by a reduction in manufacturing costs compared to other types of solar cells. The structure of PSCs involves placing the perovskite material between electron transporting material (ETM) and hole transporting material (HTM), with the ETM and HTM layers playing a crucial role in the device's overall performance. [8].

Graphene derivatives were explored to address the stability issues of perovskite cells, which are prone to instability under conditions such as moisture, ion electromigration, UV exposure, and heat decomposition. Fakelakis reported on the potential commercialization of graphene-contacted perovskite cells, emphasizing a reduction in instability through device optimization [9].

1.2 Problem Statement

The ETL is a critical component in perovskite solar cells, as it facilitates the efficient transport of electrons from the perovskite layer to the external circuit, while also preventing recombination of electrons and holes [10]. Traditional ETL materials, such as Titanium Dioxide and Zink Oxide, have limitations in terms of their cost, stability, and efficiency [11]. Graphene, with its unique combination of properties such as high electrical conductivity, optical transparency, and chemical stability, offers a promising alternative material for ETLs in perovskite solar cells. Thus, the use of graphene oxide as an ETL in perovskite solar cells aims to address is the need for high-performance, stable, and cost-effective materials for improving the efficiency and durability of perovskite solar cells [8]. The goal of investigating the use of graphene oxide as an ETL in perovskite solar cells is to develop materials and device architectures that can overcome the limitations of traditional ETLs and enable the development of high-performance and stable perovskite solar cells.

1.3 Objectives of This Project

The objectives of this research are:

i) To design perovskite solar cell with graphene oxide by using Solar Cell Capacitance Simulator-One Dimensional (SCAPS-1D) simulation software.

ii) To optimize the perovskite solar cell (PSC) device using Taguchi approach.

iii) To analyze the performance of perovskite solar cell (PSC) containing graphene oxide contacted as electron transport layer (ETL) on perovskite solar cell.

1.4 Scope of Work

First of all, study the journal, previous research and reference book as a guideline and review for more details. The literature review of this project in reference to its objective. This project combined numerical simulation using a Taguchi approach method to analyze and optimize perovskite solar cells. The Taguchi method simplifies computation, particularly when a large number of responses and parameters need to be examined at once. Predictive modeling and device simulation are the two main phases of the present effort. Solar cell capacitance simulator (SCAPS) will be used to simulate the Perovskite solar cell device [12]. Following significantly improved fill factor (FF) and power conversion efficiency (PCE), predictive modeling will be carried out to further enhance a number of device parameters. A number of the ETL layer's characteristics will be adjusted to maximize the solar cells' efficiency. The Taguchi Method is a procedure for maximizing a number of control variables that directly determine the intended or target output value. Finding the ideal control factor levels to ensure that the output reaches the desired value is the next step in the optimization process.

1.5 Thesis outline

This thesis comprises five chapters encompassing the introduction, literature review, methodology, results, and discussion, with the final chapter dedicated to concluding remarks and recommendations for the project. The first chapter sets the stage for the project by providing a comprehensive overview. It delves into the background, elucidates the project's objectives, and outlines the underlying concept. Additionally, the chapter offers a holistic perspective on the project, presenting an overall summary of its key elements.

Second chapter about the literature review of the basic structure of Perovskite Solar Cell and the effect Graphene Oxide Contacted Perovskite Solar Cell using SCAPS-1D based upon previous research.

The project's methods will be explained in the third chapter. In order to design and simulate the PSC utilizing the SCAPS-1D structure, this chapter will outline the methods and flow for problem solving in that particular technique. It will also discuss additional elements and qualities that must be considered.

The project's projected outcome is outlined in the fourth chapter, which also provides performance data to support the research archive's goals. The final chapter, which wraps up the investigation, suggests how the initiative should move forward in the future.

CHAPTER 2

BACKGROUND STUDY

2.1 Perovskite Solar Cells (PSCs)

Perovskite solar cells (PSCs) have drawn interest from academics all around the world because of its exceptional power conversion efficiency (PCE), affordable materials, and simple manufacturing procedure. These solar cells, with formula ABX_3 [A=FA (NH_2CH=NH_2), MA (CH_3NH_3); B=Pb_2; X=Cl, Br, or I], where X is a halide, have a crystal structure similar to that of calcium titanite ($CaTiO_3$) [14]. There are two types of halide perovskites: organic-inorganic halide-based, which has organic monovalent cations (A) like CH_3NH_3, $CH_3CH_2NH_3$, NH_2CHNH_2, and divalent cations (B) like Pb, Sn, Ge, and halogens X as Cl, Br, I, and F; and alkali halide-based, which has monovalent alkali cations (A) like Cs, Rb, K, Na, and Li, and divalent cations (B) like Pb, Sn, Ge, and halogens X as Cl, Br, I, and F [15]. These materials are state-of-the-art in photovoltaics because to their remarkable optical and electrical characteristics. A high absorption coefficient, a band gap that can be adjusted, a long diffusion length, minimal carrier recombination loss, and high carrier mobility are among the salient characteristics [16].

The unique properties of perovskite allow the fabrication of semitransparent solar cells, where part of the light is absorbed by the light-harvesting layer, and the rest passes through. The band gap tunability enables control over transparency by creating a thin perovskite layer. The initial photovoltaic device, based on lead halide perovskite, achieved 2.2% efficiency by Miyasaka, using CH3NH3PbBr3, with an efficiency boost to 3.8% by replacing bromine with iodine [17]. The introduction of spiro-MeOTAD as a hole-transporting material further enhanced efficiency to 9.7% in the first solid perovskite solar cells. Through advancements in thin film deposition and perovskite composition methods, PSCs reached an impressive 23% efficiency. The latest breakthrough shows a power conversion efficiency of 25.2%, as seen on the NREL PV chart. The rapid increase in PCE from 3.8% to 25.2% within a decade positions perovskite solar cells as potential replacements for widely used silicon-based solar cells. However, despite the promising results in power conversion efficiency and cost-effective fabrication, perovskite solar cells encounter challenges such as the toxicity of lead and short-term stability. The perovskite absorber layer, an ETL, and a hole transport layer (HTL) are the usual layers that make up perovskite solar cells, which have enormous potential for converting sunlight into energy. By removing electrons from the perovskite layer and moving them to the external circuit, the ETL acts as a barrier to stop electron-hole recombination, which is a critical function [18].

2.1.1 Basic Structure of Perovskite Solar Cells (PSCs)

Perovskite Solar Cells (PSCs) have a fundamental structure with several distinct layers which are substrate, Transparent Conductive Oxide (TCO), Electron Transport Layer (TCL), Electron Transport Layer (ETL), Perovskite Layer, Hole Transport Layer (HTL) and Back Contact.

Substrate is serving as the foundational layer and the substrate provides stability to the PSC. Common substrates include glass or plastic. Transparent Conductive Oxide (TCO) Layer positioned above the substrate, the TCO layer acts as a transparent electrode, facilitating the passage of light to the active layer of the solar cell. Materials like indium tin oxide (ITO) or fluorine-doped tin oxide (FTO) are commonly used for the TCO layer. Electron Transport Layer (ETL) deposited atop the TCO layer, the ETL plays a crucial role in transporting electrons from the perovskite layer to the back contact. Common materials for the ETL include titanium dioxide (TiO2) or zinc oxide (ZnO).

Perovskite layer is serving as the active layer and this layer where light is converted to electrical energy. Usually made up of methylammonium lead iodide (MAPbI3), a metal halide perovskite. Hole transport layer (HTL) is positioned above the perovskite layer. The HTL aids in the transportation of holes from the perovskite layer to the back contact. Materials like spiro-OMeTAD or PEDOT:PSS are commonly used for the HTL. Back Contact is acting as the uppermost layer, the back contact is usually a silver or gold metal electrode. It is gathering the electrons produced by the perovskite layer and makes it easier for them to leave the solar cell.

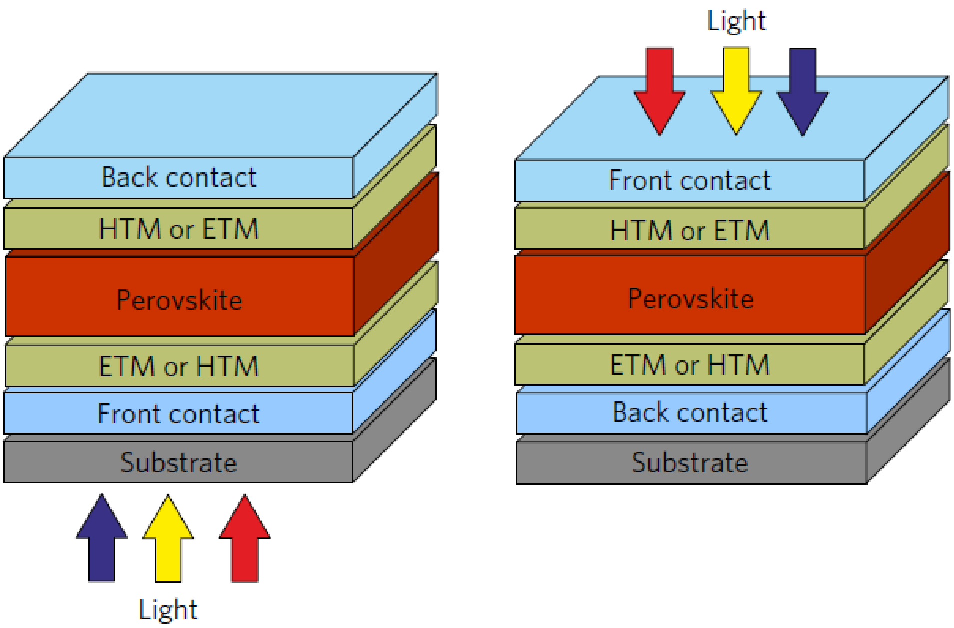

Figure 2.1: Basic structure of Perovskite Solar Cells (PSCs)

2.1.2 Research about Perovskite Solar Cells (PSCs)

Table 2.1 shows the results of PSCs in terms of Voc, Jsc, FF and power conversion efficiency (PCE) based on previous experimental research. Among the advantages, the fabrication of perovskite involves a solution process, allowing for various deposition techniques like screen printing, spin coating, and evaporation. The appeal of flexible electronics lies in their lightweight and high flexibility. In 2019, progress was made in flexible perovskite solar cells, with Huang's group achieving a record efficiency of 19.5% in single-junction perovskite solar cells, and Palmstorm's team fabricating tandem flexible perovskite solar cells with an efficiency exceeding 21%. Research from Guru Jambheshwar University of Science & Technology in India emphasizes the importance of efficient hole and electron transporting materials in designing perovskite solar cells (PSCs). Graphene, with its unique physical, structural, and electrical properties, is anticipated to positively impact the construction of PSCs [19].

Table 2.1: The Results of PSC in terms of Voc, Jsc, FF and PCE based on previous experimental research.

No.	Paper	Author	Year	Parameters			
				Voc (V)	Jsc (mA)	FF (%)	PCE (%)
1.	Simulation of perovskite solar cell with graphene as hole transporting material	Gagandeep et al.	2019	0.6992	16.92	81.86	9.64
2.	Investigating the Role of Reduced Graphene Oxide as a Universal Additive in Planar Perovskite Solar Cells	Balis et al.	2019	1.00	22.9	72%	16.5%
3.	Graphene as charge transport layers in lead free perovskite solar cell	Gagandeep et al.	2019	0.6915	19.92	77.28	10.65
4.	Design and simulation of perovskite solar cells based on graphene and TiO2/graphene nanocomposite as electron transport layer	Dadashbeik et al.	2020	0.89	21.73	82.8	16.03%
5.	Predictive Modeling of Mixed Halide Perovskite Cell Using Hybrid L27 OA Taguchi-based GRA-MLR-GA Approach	Kaharudin et al.	2021	-	-	73.11	19.41
6.	Performance analysis of carbon-based perovskite solar cells by graphene	Widianto et al.	2021	0.68	24.59	31.16	5.18%
7.	oxide as hole transport layer: Experimental and numerical simulation	Kaharudin et al.	2022	-	-	-	35.91%
8.	Optimal Modeling of Perovskite Solar Cell with Graphene Oxide HTL	Gholipoor	2022	0.928	-	89%	20.32%

In 2020, Mehran et al. utilized a three-dimensional finite element method (FEM) technique. The use of monolayer graphene as the electron transport layer (ETL) enhanced absorption in the active layer, increasing Jsc from 19.07 to 21.73 mA/cm^2. The introduction of a TiO_2/graphene nanocomposite as the ETL improved carrier transport, increasing Voc from 0.99V to 1.15V. The PCE in the optimal case (TiO2/Gr (10%) nanocomposite) reached 17.01%. Additional enhancements were explored by incorporating three different hole transport layers (HTLs) – CuSCN, Cu2O, and NiO – resulting in increased PCEs of 17.01%, 17.81%, and 17.94%, respectively [6]. In 2022, replacing the reduced graphene oxide (rGO) layer with a Spiro-OMeTAD layer as a hole transport layer (HTL) led to improvements. The Open Circuit Voltage (VOC) increased from 0.84 to 0.928 V, and the Process Cycle Efficiency (PCE) rose from 18.52% to 20.32%. This highlights the effective performance of the rGO layer as both an interlayer and charge transport layer in PSCs [20].

2.1.3 Advantage of Perovskite Solar Cells (PSCs)

Here are some advantages and benefits of perovskite solar cells, including optimum efficiency, economical manufacturing, versatility and flexibility, adjustable optical and electrical and swift technological advancements. PSC have rapidly achieved noteworthy levels of power conversion efficiency (PCE). Surpassing many thin-film solar cell technologies, they hold the potential to match or even exceed the efficiency of traditional silicon-based solar cells. In economical manufacturing, perovskite solar cells can be manufactured at a low cost by utilizing cost-effective solution-based techniques like spin-coating, inkjet printing, or spray deposition. This opens up possibilities for scalable and budget-friendly production, making them economically viable for large-scale deployment.

Perovskite solar cells also can be produced on various substrates, including flexible and lightweight materials like plastics. This adaptability creates opportunities for integration into diverse applications, such as curved surfaces, portable electronics, building-integrated photovoltaics (BIPV), and wearable devices. Meanwhile, their optical and electrical properties can be fine-tuned through modifications in the chemical composition of perovskite materials. This flexibility enables researchers to optimize the bandgap and optical characteristics, enhancing sunlight absorption and potentially achieving higher efficiencies. In swift technological advancements, the field of perovskite solar cell research has experienced rapid progress, marked by frequent breakthroughs in materials, device architectures, and manufacturing techniques. This dynamic nature holds the promise of ongoing improvements and the potential for commercialization in the future.

2.2 Graphene Oxide (GO)

Graphene oxide (GO) is a unique substance that has the appearance of a single monomolecular graphite sheet and is composed of different oxygen-containing functions such as hydroxyl, carbonyl, carboxyl, and epoxide groups. Reduced graphene oxide (rGO), which resembles graphene but retains residual oxygen, other heteroatoms, and structural flaws, is created by an appropriate reduction procedure. Both GO and rGO have uses in catalysis, energy storage, polymer composites, nanocomposite materials, and biological applications. These domains frequently overlap. Moreover, graphene-based applications in electronics, optics, chemistry, energy storage, and biology show promise for GO as a material. Commercial solar cells have a power conversion efficiency (PCE) of between 10 and 22 percent when using different light absorbers; however, the development of thin-film solar cells is expected to benefit from graphene's special structural, physical, and electrical features.

The possibility of using graphene as an active interfacial layer and front and back connections in the creation of solar cells is still being investigated [21].

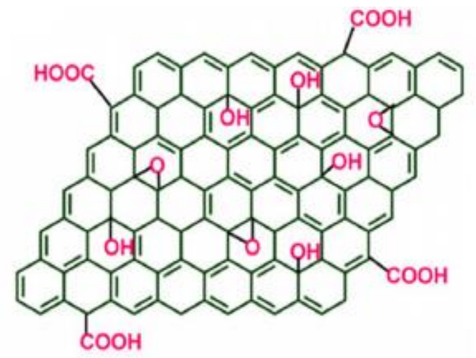

Figure 2.2: Graphene oxide (GO)

2.2.1 The function of graphene oxide (GO) in ETL layer of Perovskite Solar Cells (PSCs)

With their ability to convert sunlight into electrical power, perovskite solar cells are very promising. They are usually made up of three layers: an ETL, a hole transport layer, HTL, and a perovskite absorber layer. By collecting and moving electrons from the perovskite layer to the external circuit and acting as a barrier to stop electron-hole recombination, the ETL is essential. Graphene oxide emerges as an appealing candidate for the ETL in perovskite solar cells due to its noteworthy properties. It boasts excellent electrical conductivity, a substantial surface area, and favorable optical transparency qualities highly desirable for an ETL. Furthermore, graphene oxide exhibits chemical stability and mechanical robustness, potentially enhancing the long-term stability of the solar cell device.

2.3 SCAPS (Solar Cell Capacitance Simulator)

A one-dimensional solar cell simulation tool called SCAPS (Solar Cell Capacitance Simulator) was created by the University of Gent's Department of Electronics and Information Systems (ELIS) in Belgium. One-Dimensional Solar Cell Capacitance Simulator (SCAPS-1D) is a software program used to simulate the electrical behavior and operation of solar cells. Figure 2.3 shows the interface of SCAPS-1D tools. With parameters like material properties, device structure, and operating conditions, SCAPS-1D allows researchers and engineers to simulate the electrical characteristics of solar cells. It is specifically designed for one-dimensional (1D) devices like thin-film solar cells, including perovskite solar cells (PSCs) [22]. Significant measurements including current-voltage (I-V) and capacitance-voltage (C-V) characteristics are computed by the software, providing insightful information on the functionality and behavior of the device.

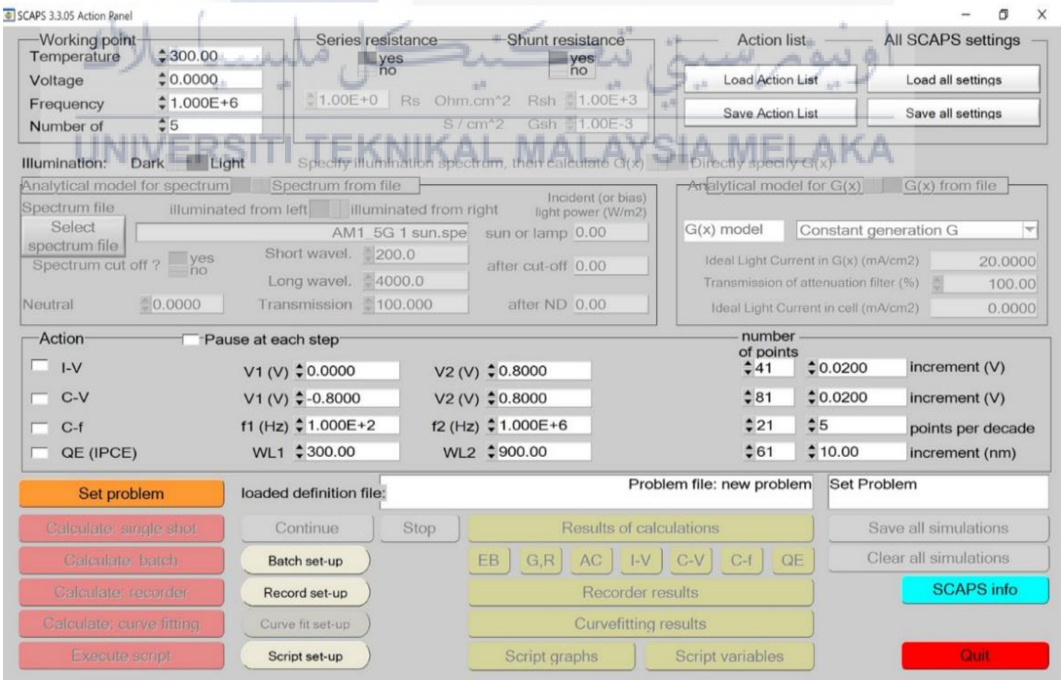

Figure 2.3: Interface of SCAPS-1D Tools

These are SCAPS-1D's salient characteristics such as device modeling, physical models, parameter extraction, interface characterization and sensitivity analysis. SCAPS-1D provides a platform that allows users to define the device's modeling and architecture, including the many interfaces and layers inside the solar cell. Important factors including material characteristics, thicknesses, doping concentrations, and other relevant data can be entered by users. Meanwhile, to faithfully reproduce the electrical characteristics of solar cells, the software makes use of a variety of physical models. These models consider factors that affect the device's performance, including carrier transport, recombination, optical absorption, and other phenomena. In parameter extraction, SCAPS-1D has the capability to extract material parameters from experimental data, such as recombination lifetimes, carrier mobilities, and trap densities. These parameters can then be utilized to improve the device simulations' optimization.

In interface characterization section, it is easy to characterize the interfaces between different layers in the solar cell, such a tool allows users to investigate how interface characteristics affect the device performance. SCAPS-1D also provides the ability to conduct sensitivity analysis, aiding in the identification of crucial parameters that have a significant impact on the performance of the solar cell. This empowers researchers to comprehend the behavior of the device and optimize its efficiency.

In conclusion, SCAPS-1D finds extensive use in the photovoltaics field for simulating and analyzing diverse solar cell technologies, including perovskite solar cells. It offers valuable insights into performance limitations, efficiency enhancements, and the optimization of solar cell designs, contributing to the creation of more efficient and dependable devices.

2.4 Taguchi Method

Dr. Genichi Taguchi invented the Taguchi method which has shown to be a useful tool in a number of engineering disciplines. The Taguchi approach is based on a strategy that is entirely unlike from the traditional methods of quality engineering. The technique places a greater emphasis on incorporating quality into goods and processes than does customary practice which focuses on inspection. Taguchi essentially used normal statistical methods, but simplified it by referring them as a set of rules for organizing experiments and analyzing the results. The Taguchi experimental design technique is appropriate for a variety of applications involving several variables [22].

For the best PSC device performance, every device modelling must include optimization techniques. One of the key industrial processes to enhance product performance and reduce production costs is the optimization of manufacturing processes and products. Utilizing an optimization strategy for designing experiments based on Taguchi method is a methodical and effective way to do. In these situations, Taguchi method offer the most effective and practical answer with the fewest number of experimental trials [12].

The Taguchi method is used to discover the material electrical properties whose fluctuation would have the greatest influence on the device characteristics. This technique has evolved into a supreme tool for increasing research and development productivity so that high-quality solutions may be created swiftly and affordably. The approach yields ideal electrical settings that are insensitive to changes in the outside environment and other noise sources. With just a few tests, this approach studies the whole process parameter space using a unique design of orthogonal arrays. An orthogonal array might be used to quickly and cheaply evaluate the effects of various controllable factors on the average of quality features and the variances in the experiment [23].

2.4.1 Orthogonal Array

A general fractional factorial design is the Taguchi Orthogonal Array (OA) design. Based on a design matrix suggested by Dr. Genichi Taguchi, it is a highly fractional orthogonal design that enables to take into account a certain subset of combinations of various aspects at various levels. To ensure that all levels of each factor are taken into account equally, Taguchi orthogonal arrays are fairly balanced. Because of this, despite the rationality of the design, the elements can be assessed independently of one another [24].

The use of Orthogonal Arrays (OA) in the design is one of the Taguchi method's key benefits for optimization. The job of planning experiments is significantly reduced by orthogonal arrays (OA), especially when there are several experiments runs. The Taguchi techniques assist in minimizing the quantity of experiments needed for optimization [23].

2.4.2 Experiment Design Strategy

A unique collection of orthogonal arrays (OAs) is used to build the Taguchi technique in order to lay out various trials. A sample OA for three-level factors is shown in Table 2.1. This array which is called the L_9 design is used to create experiments with up to four 3-level components. There are four columns and nine rows in the array. The numbers in each row show the factor levels in each trial experiment. The factors listed in the research are reflected in the vertical columns. For the factor allocated to the column, each column comprises three level 1, three level 2, and three level 3 conditions. It follows that there are an equal number of levels in each column. As a result, the four columns at a given level are all orthogonal to one another [23].

Table 2.2: Taguchi Method Experiment Design

Experiment No.	Control Factor			
	A	B	C	D
1	1	1	1	1
2	1	2	2	2
3	1	3	3	3
4	2	1	2	3
5	2	2	3	1
6	2	3	1	2
7	3	1	3	2
8	3	2	1	3
9	3	3	2	1

The experiment design process is made easier by the OA. It is crucial to choose the most appropriate orthogonal array when constructing an experiment, allocate the elements to the proper columns, and then explain the combinations of individual trials known as trial experiments. All experimenters are compelled by the array to create almost similar experiments. The nine trial runs will contain all combinations regardless of the column definitions that the experimenters choose for the columns. As a result, OA ensures that various experimenters' designs are consistent [12].

In the context of this research, optimization of all parameters for Perovskite Solar Cells is essential to achieve optimal performance. Optimizing manufacturing operations and products is crucial for enhancing product performance and reducing manufacturing costs. The Taguchi method, with its systematic and efficient approach to designing experiments, proves to be highly effective in such cases, requiring minimal experimental trials to achieve the desired results.

CHAPTER 3

METHODOLOGY

For this chapter contain how to use the data and information gathered using a certain technique to acquire and achieve the project's objectives. This section also includes the key flowchart for this concentration in order to make the task embraced clearer and methodically based in order to achieve better and better results. This part will provide an overview of the technique that will be used, which will cover the complete scope of this project.

3.1. Overview

This analysis has two part which is simulation and optimization the result using Taguchi method. The simulation part is carried out by using SCAPS-1D software where the solarstructure of PSC is simulated initially to analyze the optimum efficiency. The PSC structure is investigated in various aspects including the the different materials as ETL, thickness of perovsikte layer, the defect density, capture cross section electrons and holes. From SCAPS-1D the I-V characteristics are used to evaluate the PCE, FF, Voc and Jsc. Then after collect all the data, optimize the data using Taguchi method in order to obtain the effective result.

3.2. Flowchart of the project

In this project, there are a few methods that have been carried out to obtain the desired results. Figure 3.1 shows the overall flowchart of the project.

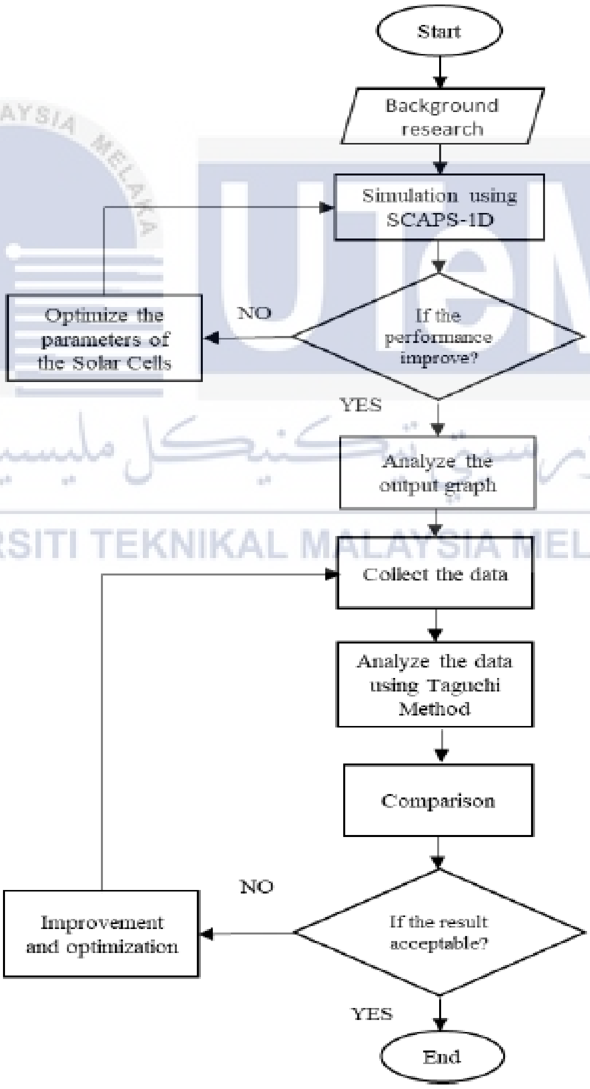

Figure 3.1: Overall flowchart of the project

Meanwhile, Figure 3.2 shows the overall method and entire flow for this project. The methods for this project are divided into 3 phases. The details for each phase are explained in this section.

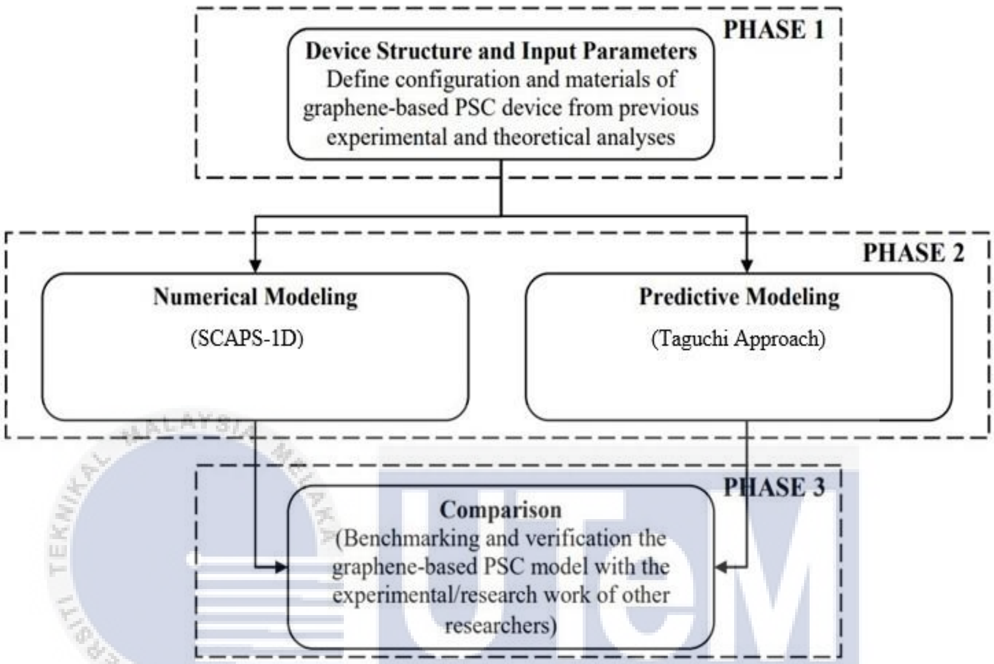

Figure 3.2: Indetails flowchart of the project

In phase 1, different ETL materials will be tested later to find the best materials that maximize the cell performance. To find the best ETL materials, more simulations need to be conducted following the same approach with a variety of materials for ETL. Key simulation parameters for the PSC device will be obtained from previous experimental and theoretical analyses.

There are two types of modeling will be performed which are numerical modeling and predictive modeling. In phase 2, after reviewing past researches that have been carried out, both numerical and predictive modeling of the PSC device should be ready to be performed. The main difference between numerical and predictive modeling is that the numerical modeling purely relies on numerical approach performed via software such as SCAPS software, whereas the predictive modeling relies on the combination of both, numerical and predictive approaches such as statistic, machine learning and artificial intelligent.

In phase 3, for verification, the performance of the PSC device with different ETL materials and the performance of the PSC with the proposed ETL materials will be compared. The simulation results of PSC devices obtained from the proposed material will be identified and compared with the experimental/research work of other researchers. It will also summarize the benchmark for this project.

3.3 Flowchart of Taguchi Method

This project utilized the Taguchi method to determine the optimal solution for PSCs devices. Taguchi also is statistical methods to improve the quality of manufactured goods that applied in engineering and many other field. Taguchi method emphasizes the design and execution of experiments that can determine the effect of input process parameters on output responses. By analyzing the impact of different components, the optimal combination of factors can be identified. Figure 3.3 depicts the primary implementation processes for Taguchi method input process parameter optimization.

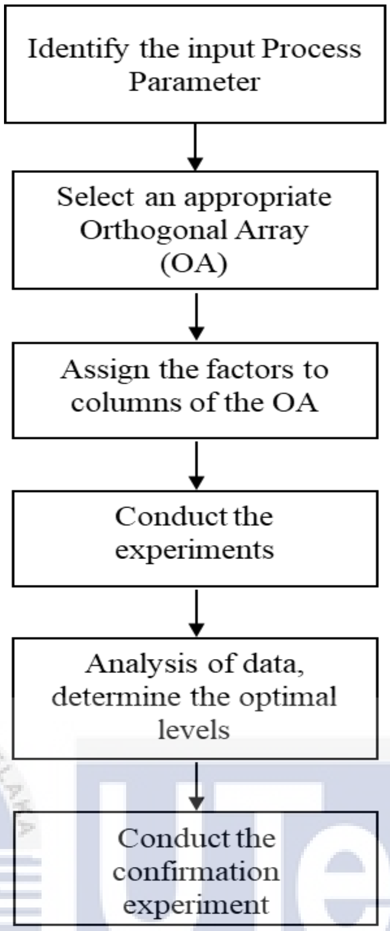

Figure 3.3: Optimization Approach Using Taguchi Method

3.2 Numerical Modeling for Device Simulation

There are several steps in running a simulation such as setting the problem, providing important parameters and need to be followed by configuring the working conditions such as temperature and spectrum. Next is to determine the desired output size and finally to perform the simulation. The sequence for starting a simulation with SCAPS is very simple but comprehensive.

3.2.1. SCAPS-1D

SCAPS-1D is numerical modelling simulation tool up to seven semiconductor layers developed by a photovoltaic researcher at the University of Gent's Department of Electronics and Information Systems. For solar cell devices with up to seven semiconductor layers, SCAPS-1D extracts the electrical parameters such as acceptor and donor density, current densities and so on. Solving the Poisson equation in Equation (3.1) and the continuity equations for electrons and holes in Equations (3.2) and (3.3) respectively. These equations contained in the programmed provides the spectrum response of solar radiation and current-voltage (J-V) characteristics [25].

$$\frac{d}{dx}\left[\varepsilon(X)\frac{d\Psi}{dx}\right] = q[p(x) - n(x) + N_D^+(x) - N_A^-(x) + p_t(x) - n_t(x)] \quad (3.1)$$

$$-\frac{1}{q}\frac{dJ_n}{dx} + R_n(x) - G(x) = 0 \quad (3.2)$$

$$\frac{1}{q}\frac{dJ_p}{dx} + R_p(x) - G(x) = 0 \quad (3.3)$$

Where, Ψ = electrostatic potential, ε = dielectric permittivity (relative), x = denotes the position, $\mathbf{N_A}$ = ionized acceptor, $\mathbf{N_D}$ = ionized donor, p = holes, e = electrons, $\mathbf{P_t}$= number of trapped holes, $\mathbf{n_t}$ = number of trapped electrons, $\mathbf{J_p}$ = holes current density, $\mathbf{J_n}$ = electrons current density, G(x) = generation rates, $\mathbf{R_p}$ (x) = recombination rate of holes and $\mathbf{R_n}$ (x) = recombination rate of electrons. It allows the user to modelthe bandgap energy diagram and the I-V curve of a solar cell by constructing a p-n junction, adding contacts, and simulating the bandgap energy diagram and I-V curve. SCAPS is a simple application that may be used for both research and education. Meanwhile, Figure 3.4 shows the working point and lighting are set on the action panel of SCAPS.

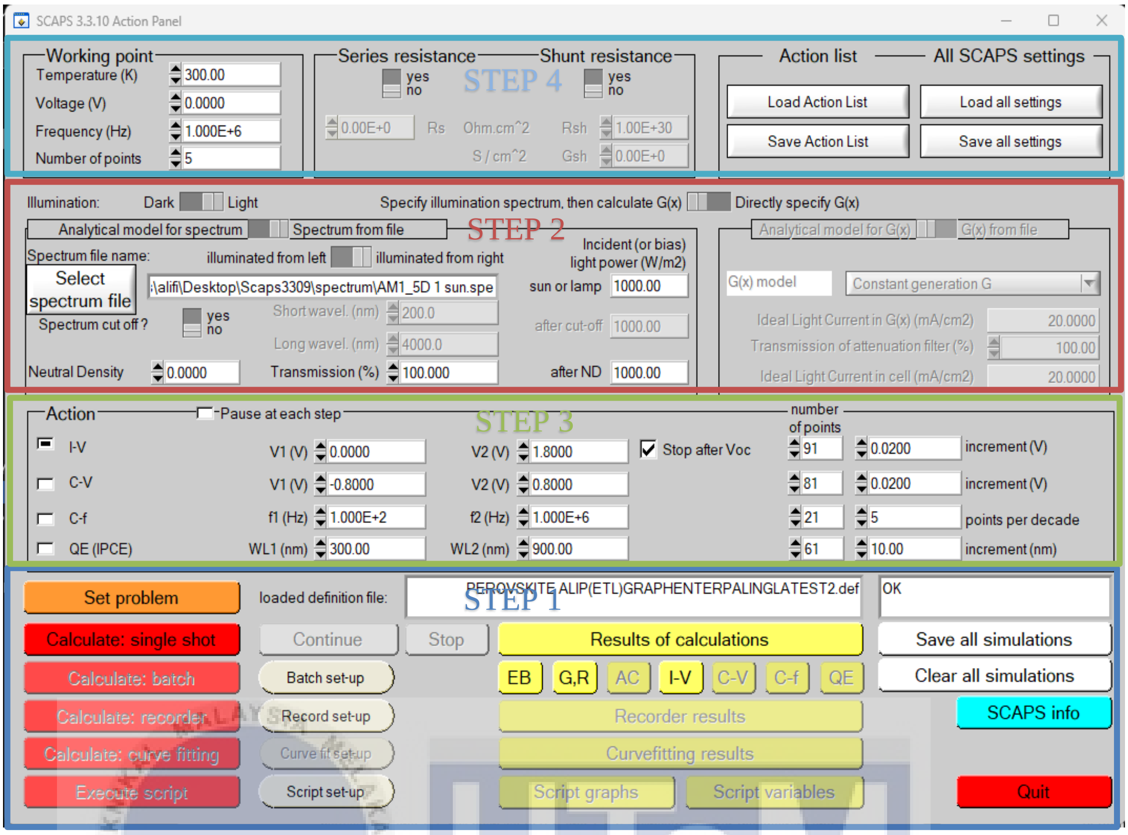

Figure 3.4: SCAPS-1D Action Panel

In SCAPS-1D, the set problem is used to design each layer of solar cell structure, to insert electrical parameter, and add interfaces between layers. The action setting is used to show the client which estimation of the sun-powered cell to reproduce. I-V quality scale adjustment, C-V capacitance voltage adjustment, C-f capacitance recurrence adjustment, and QE quantum productivity adjustment are all included. In this experiment, only the I-V configuration will be used to determine the Power Conversion Efficiency (PCE). The solar cell's scope, which is somewhere between V1 and V2, has been set to 0 V and 1.8 V, respectively. For the diagram and boundary of the solar cell to be shown after executing the application, this reach needs be set at a specific value. The illumination setting is used to set the range and the course of the prevailing light condition, which can be dull or bright. The daylight was adjusted to a standard brightness of AM1.5G, 1000W/m^2 and the light in the enlightenment settingwas turned on. Before calculating single shot need to set the temperature of the sunlight intensity. The temperature can set in kelvin unit.

3.2.2. SCAPS-1D problem setting

Figure 3.5 shows the SCAPS-1D software and it consists of four settings. After clicking on set problem, as shown in Figure 3.5, the solar cell defining board is opened. There are three classifications on this board and five buttons on it. These buttons have the ability to create new, load, and save construction records in the SCAPS definition library. The layers of the solar cell are saved as '.def' files. After characterizing the design, the 'ok' button is pressed.

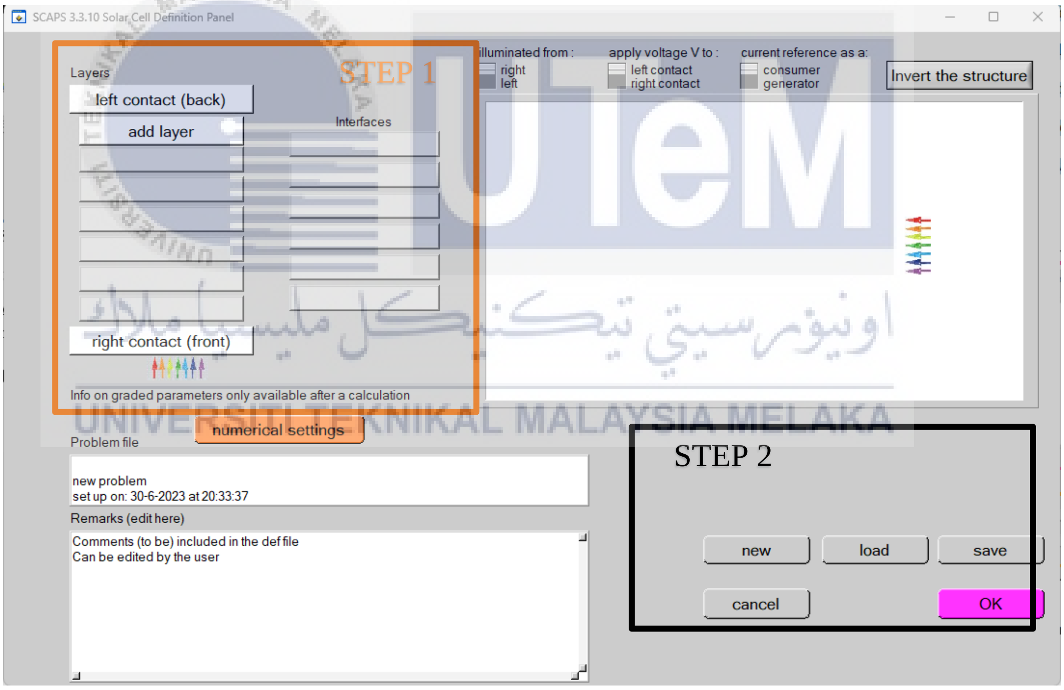

Figure 3.5: SCAPS-1D Solar Cell Definition Panel

3.2.3. SCAPS-1D adding layers to structure

Figure 3.6 to Figure 3.9 show the setting layer and these figures consist of interface between layer, back and front contact and mathematical inclinations. The SCAPS-1D can only assist in the creation of a sun-powered cell with up to 7 layers. In this segment it can change the position of illuminated from left or right. A few buttons are used to applied voltage and current. It also can see the thickness and the color each layer of solar cell. In this SCAPS-1D layer properties board are used to insert the electrical parameter each of the material. The mathematical examination boundaries for each layer in PSC devices are based on the SCAPS –ID input parameter from previous researchers as shown in Table 3.1 and Table 3.2 [26,12,27,28].

Table 3.1: SCAPS-1D Input Parameter of Numerical for Each Layer in PSC Devices

Parameters	MATERIALS			
	FTO	GO	$CH_3NH_3PBI_3$	Cu_2O
Thickness, d (nm)	50	50	300	400
Bandgap, Eg(ev)	3.5	2.2 [16]	1.55	2.170
Electron affinity χ (ev)	4	3.9 [18]	3.93	3.200
Dielectric permittivity ε_r	9	6.9	6.5	7.110
CB effective density of states, N_C (cm^{-3})	2.2×10^{18}	1×10^{19}	2.2×10^{18}	2.0×10^{17}
VB effective density of states, N_V (cm^{-3})	1.0×10^{19}	1×10^{19}	1.0×10^{19}	1.1×10^{19}
Electron thermal velocity (cms^{-1})	1.0×10^7	1×10^7	1.0×10^7	1.0×10^7
Hole thermal velocity (cms^{-1})	1.0×10^7	1×10^7	1.0×10^7	1.0×10^7
Electron mobility, u_n	20	9000	0.5	200
Hole mobility, u_p	10	9000	0.5	80
Donor density, N_D (cm^{-3})	2.0×10^{19}	5.0×10^{18}	-	-
Acceptor density, N_A (cm^{-3})	-	-	1.0×10^{13}	1.0×10^{18}
Defect GO/$CH_3NH_3PBI_3$	-	-	1.0×10^{14} [17]	1.0×10^{14}

Table 3.2: The Parameters of the Interface Defect of ETL/Perovskite [27]

Parameters	ETL/Perovskite
Defect type	Neutral
Capture cross-sections electrons (cm^2)	1×10^{-15}
Capture cross-sections holes (cm^2)	1×10^{-15}
Energetic distribution	Single
Reference for defect energy level E_t	Above the highest EV
Energy with respect to a reference (eV)	0.600
Total density (cm^{-2})	10^{14} (variable)

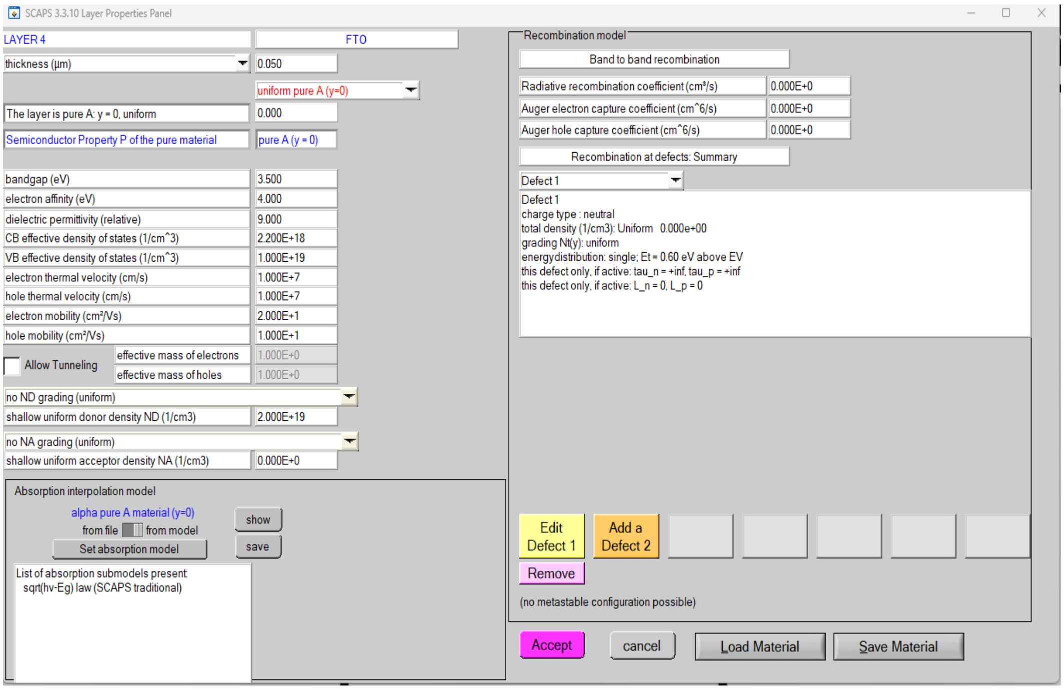

Figure 3.6: SCAPS-1D Layer Properties Panel For TCO Layer

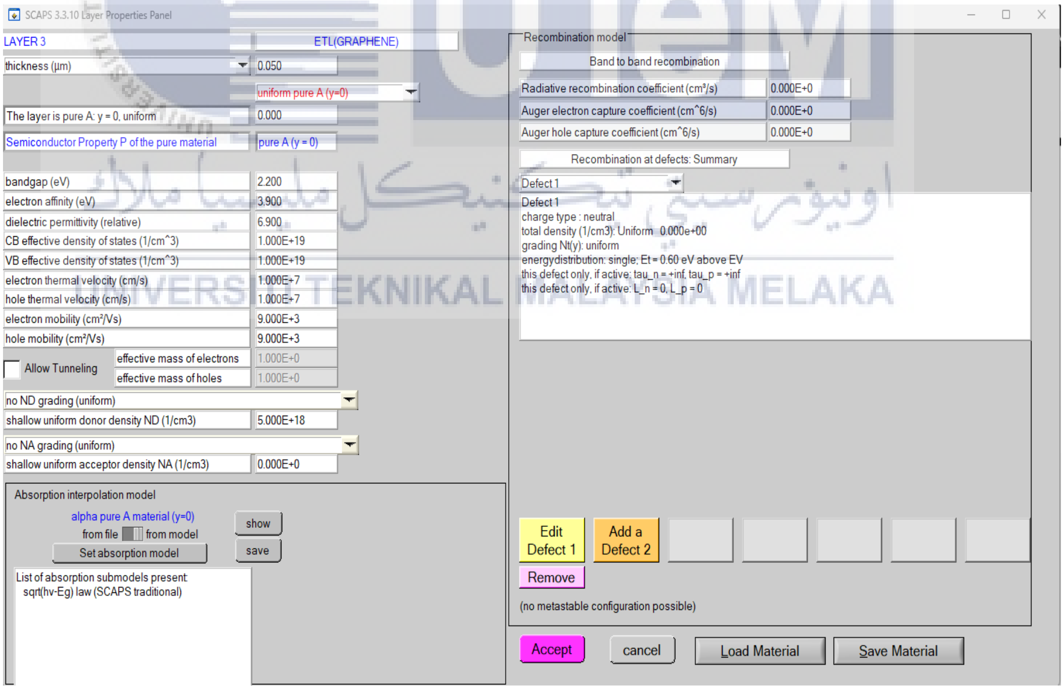

Figure 3.7: SCAPS-1D Layer Properties Panel For ETL Layer

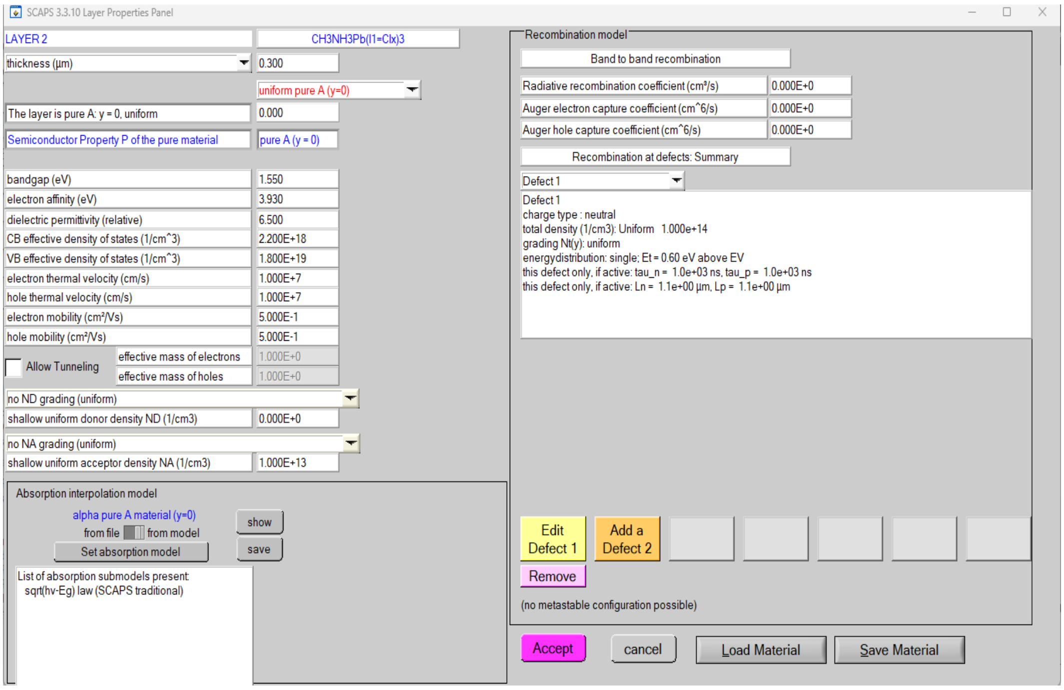

Figure 3.8: SCAPS-1D Layer Properties Panel For Perovskite Layer

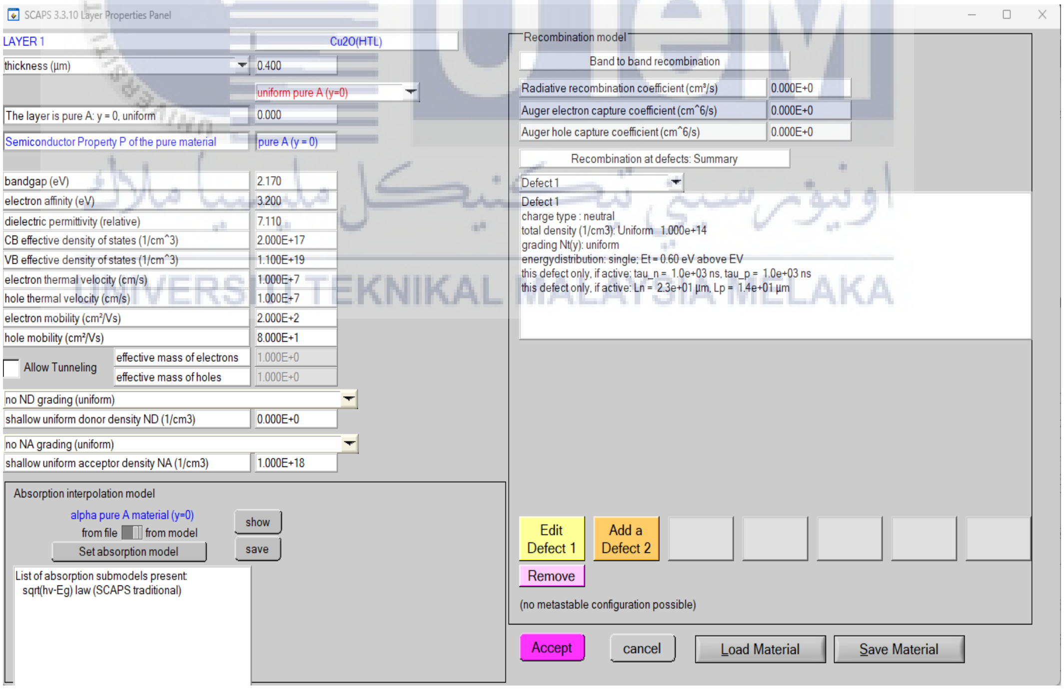

Figure 3.9: SCAPS-1D Layer Properties Panel For HTL Layer

3.2.4. SCAPS-1D simulation for PSC with GO as ETL

In this experiment, there are five layers in the PSC device. First layer is FTO function as front contact where the metal work function for FTO is 4.0eV. Then followed by GO as the ETL, the active layer which is perovskite, CH3NH3PBI3, Cu20 as HTL and Ag as back contact where the metal work function for Ag is range from 4.26-4.73eV. There are 4 parameters have been optimized to obtain optimal effectiveness of PSC device based on the presence of GO as ETL. The parameters are the thickness of provskite, capture cross section electrons, capture cross section holes and defect density of perovskite. Tables 3.1, 3.2 and 3.3 show the numerical analysis input parameter for each component mentioned in the previous research.

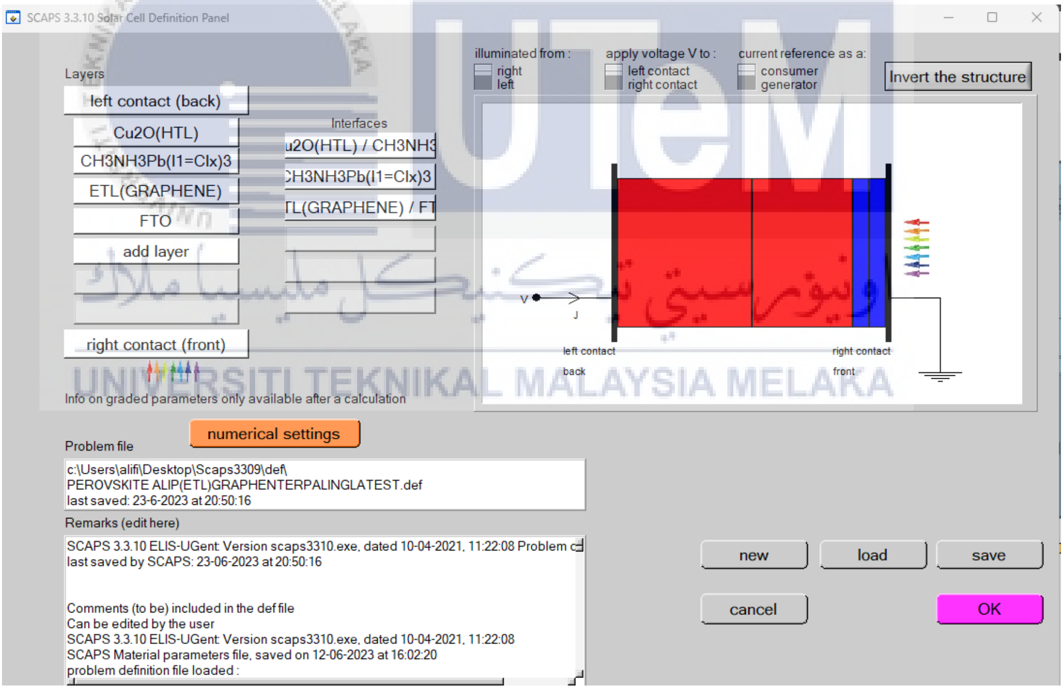

Figure 3.10: Simulated device structure of PSC of GO as ETL

Finally, after simulation, the I-V curve will be analyzed and see the performance of IPSC through PCE. From I-V curve it shows the Voc, Jsc, FF and PCE. In any case, if the results do not match the ideal result, the method should be reviewed until the ideal result is achieved

Table 3.3: SCAPS-1D Input Parameter of Numerical for Each Difference Material of ETL Layer in PSC Devices [26,12]

Parameters	ETL MATERIALS				
	TIO	TIO_2GO (5%)	TIO_2GO (10%)	TIO_2GO (20%)	ZnO
Thickness d (nm)	50	50	50	50	40
Bandgap Eg (ev)	2.2	3.1	2.7	2.170	3.3
Electron affinity χ (ev)	3.9	4.24	4.28	3.200	3.9
Dielectric permittivity ε_r	6.9	7.3	6.5	7.110	9
CB effective density of states N_C (cm^{-3})	1.0×10^{19}	1×10^{19}	1×10^{19}	1×10^{19}	1×10^{19}
VB effective density of states, N_V(cm^{-3})	1.0×10^{19}	1×10^{19}	1×10^{19}	1×10^{19}	1×10^{19}
Electron thermal velocity	1.0×10^{7}	1×10^{7}	1×10^{7}	1×10^{7}	1×10^{7}
Hole thermal velocity	1.0×10^{7}	1×10^{7}	1×10^{7}	1×10^{7}	1×10^{7}
Electron mobility, u_n	9000	12	125	350	50
Hole mobility, u_p	9000	12	125	350	5
Donor density, N_D (cm^{-3})	5×10^{18}	5.0×10^{18}	5.0×10^{18}	5.0×10^{18}	5.0×10^{17}
Acceptor density, N_A (cm^{-3})	-	-	-	-	-
Defect Density, Nt (cm−3)	-	-	-	-	1.x 10^{16}

3.5 Taguchi Method

In this experiment, PSC parameters should meet the performance specification such as Voc, Jsc, FF and PCE. One of the statistically methods for identifying the parameters, whose variability affect the effect of the PSC performance is Taguchi method. Taguchi method has become a powerful tool for improving productivity during research and development. Taguchi method also can improve the quality of the analyzed processes and products. The increment the number of process parameters, many experiments need to execute. The Taguchi method employs a unique design of orthogonal arrays to address this issue and explore the whole process parameter space with just a few experiments. The PSC as GO as ETL optimization process flow is depicted in Figure 3.2.

3.5.1 Selection of Orthogonal Array

Orthogonal array (OA) can reduce the number of experimental. In order to choose an appropriate orthogonal array (OA) it depends on the total of parameter. In these experiments, L9 OA was used and it has 9 experiments with 4 control factors. Taguchi L9 OA greatly can reduce the number of tests and increase the efficiency. The experimental layout for the process parameters employing an orthogonal array of L9 (3^4) elements. The L9 orthogonal array is used to comprehend the effect of four controlfactors whose levels were altered throughout nine rows of experiments.

Table 3.4: Experimental Layout Using L9 (3^4) Orthogonal Array

Expt. No.	Control Factors				S/N Ratio (dB)
	A thickness of perovskite layer	B capture cross section electrons in perovsikte layer	C Capture cross section of holes in perovsikte layer	D defect density of perovskite layer	
1	1	1	1	1	η_1
2	1	2	2	2	η_2
3	1	3	3	3	η_3
4	2	1	2	3	η_4
5	2	2	3	1	η_5
6	2	3	1	2	η_6
7	3	1	3	2	η_7
8	3	2	1	3	η_8
9	3	3	2	1	η_9

3.5.2 Larger is Better

The target is to maximize the respond. The bigger the S/N, the better it is calculated to be. Since our aim is to maximize strength, the compressive strength in the current study should be higher. Equation (3.4) shows the Ƞ for the quality characteristics of higher-the-better. The number of tests and experimental value of the obtained respond characteristics being represented as n and Yn respectively [29].

$$\eta = -10 \log_{10} \left[\frac{1}{n} \Sigma \left(\frac{1}{Y1*2} + \frac{1}{Y2*2} + \cdots + \frac{1}{Y3*3}\right)\right] \tag{3.4}$$

Experimentation can be utilized, for instance, to examine the influence of Factor A at level 3 (A_3). Level A_3 of factor A was observed in experiments 7, 8, and 9. The average S/N ratio for these experiments, denoted by, mA_3 is calculated as follows [29].

$$M_{A3} = \frac{1}{3} [\eta_7 + \eta_8 + \eta_9] \tag{3.5}$$

Therefore, ($mA3-m$) from Table 3.4 represents the effect of Factor A at level A3. For forexperiments 7, 8, and 9, the level of Factor B is 1, 2, and 3, respectively. In a similar vein, during these studies, Factors C and D's levels have the numbers 1, 2, and 3. As a result, when the perovskite layer thickness is at level A3, the amount $mA3$ represents an average, and the averaging is carried out in a balanced manner across all levels of the other three components. The same method can be used to compute the average S/N ratio for Factor A's levels A1 and A2, as well as the ratios for the various levels of the other components.

$$M_{B3} = \frac{1}{3} [\eta_2 + \eta_5 + \eta_8] \tag{3.6}$$

The mean S/N ratio for Factor B at level B2. All level averages have the same balancing property as m*A*3 since the matrix experiment is constructed on an orthogonal array.

3.5.3 Confirmation Experiment

In this experiment, initially 4 control factors were selected and L_9 orthogonal array was used. The confirmation experiment is the last phase in the process of designing an experiment. Verifying the analysis phase's conclusions is the goal of the confirmation experiment [30]. To verify the correctness of the Taguchi Method prediction, a final simulation or confirmation test is run after the ideal level of process parameters has been established. If one of the experiments in the orthogonal array coincides with the ideal combination of parameters and their levels, the confirmatory test is not required. By adding the average performance to the contribution of each parameter at the optimal level, one can calculate the estimated value of the response characteristic under ideal conditions using the following equations [31]:

$$Y_{opt} = m + \sum_{i=1}^{n} (m_{iopt} - m) \tag{3.7}$$

Where n is the number of process parameters or control variables, m is the average performance, and miopt is the average process parameter at the optimal level.

CHAPTER 4

RESULT AND ANALYSIS

In this chapter will discuss the outcome that has been successfully obtained from the simulation process in this project. Different parameters have been analyzed using Taguchi method L_9 (OA) and the results will be discussed to obtain a better performance of the device. Then, all the parameters will be related with theory and discussed regarding problems faces during an experiment.

4.1 Analysis of Different ETL Materials in PSC

Analyzed the different ETL materials in PSC in order the improved the performance of PSC. Initially, there are many materials that can be used as ETL on PSC such as ZnO, TIO_2, GO and more else. For this part, GO has been focused in order to analyst it's performance as ETL layer in PSC. As shown in Table 4.1, from the simulation result, PCE values of the different material that has been used is around 18.13% to 19.65%. GO has the highest PCE at 19.65%, while TIO_2 GO (20%) has the lowest at 18.13%. This indicates that GO performs slightly better in terms of power conversion efficiency compared to the other materials. For, fill factor values are quite consistent across the materials, ranging from 81.06% to 84.77%. GO has the highest FF at 84.77% compared to the other results. While, for Voc which is open circuit voltage, the values vary slightly, with the highest at 1.2095 V which is G) and the lowest at 1.1690 V which is the combination of TIO_2 and GO (20%). GO has the highest Voc, indicating its potential for higher voltage output in the solar cell. Lastly, for Jsc, short circuit current, the values are relatively consistent across materials, with a narrow range from 19.1 mA to 19.16 mA, and still the GO has the highest value of Jsc, which is 19.16 mA.

Table 4.1: Comparison of Different ETL Materials Performance [6,12]

Different ETL Materials	PCE (%)		FF (%)		Voc (V)		Jsc (mA)	
	Previous research	Simulation	Previous research	Simulation	Previous research	Simulation	Previous research	Simulation
GO	16.03	19.65	82.8	84.77	0.89	1.2095	21.73	19.16
ZnO	19.41	19.58	73.11	84.75	0.83	1.2082	29.64	19.12
TIO_2	14.42	19.37	76.3	84.00	0.99	1.2062	19.07	19.12
TIO_2 GO (5%)	14.93	19.07	82.1	83.20	1.05	1.1985	17.32	19.12
TIO_2 GO (10%)	17.01	18.58	84.3	81.97	1.14	1.1850	17.69	19.12
TIO_2 GO (20%)	16.47	18.13	83.7	81.06	1.15	1.1690	17.10	19.1

In summary, GO seems to perform slightly better in terms of PCE and Voc, FF and Jsc values from the other ETL materials.

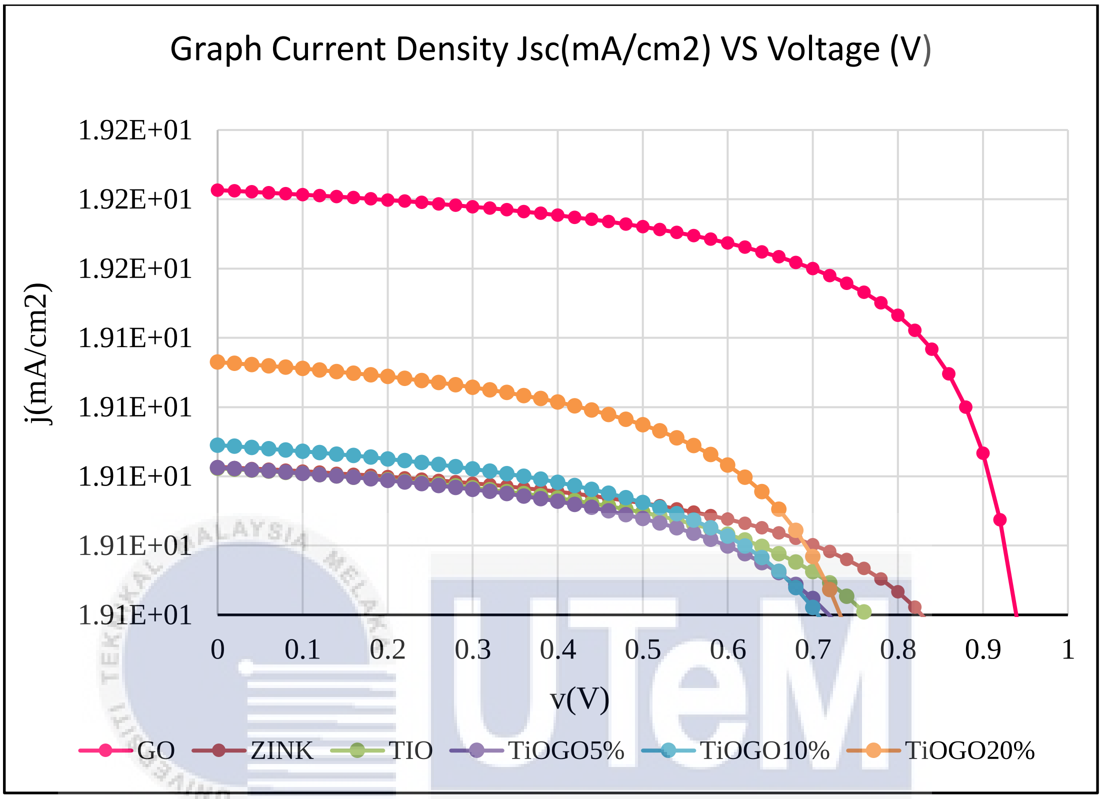

Figure 4.1: The Graph Jsc vs Voc with different material as ETL in Perovskite

From Figure 4.1, the graph is about short circuit current Jsc vs open circuit voltage open circuit Voc for the simulation of different ETL materials such as GO, ZnO, TIO_2 and combination of TIO_2 and Graphene, from the trend line of graph, GO has the most stable and relatively high conductivity across the voltage range from the other materials. Thus, it proves that graphene is the best material as the ETL of PSC in order to get the better performance in term of PCE and Voc, FF and Jsc.

4.2 Analysis of Thickness of Perovskite Layer

For this part, the thickness of Perovskite layer has been analyzed to improve the performance of PSC. Initially, the thickness of perovskite layer varied from 100 nm to

300 nm as be shown on Table 4.2. The trend of a varied thickness of Perovskite layer for four parameters which is PCE, FF, J_{sc} and V_{oc} is illustrated in Figure 4.2

Table 4.2: The Range of Thickness of Perovskite Layer

Thickness of perovskite layer (nm)	PCE (%)
100	13.68
120	14.6
140	15.44
160	16.19
180	16.85
200	17.45
220	17.99
240	18.48
260	18.92
280	19.3
300	19.65

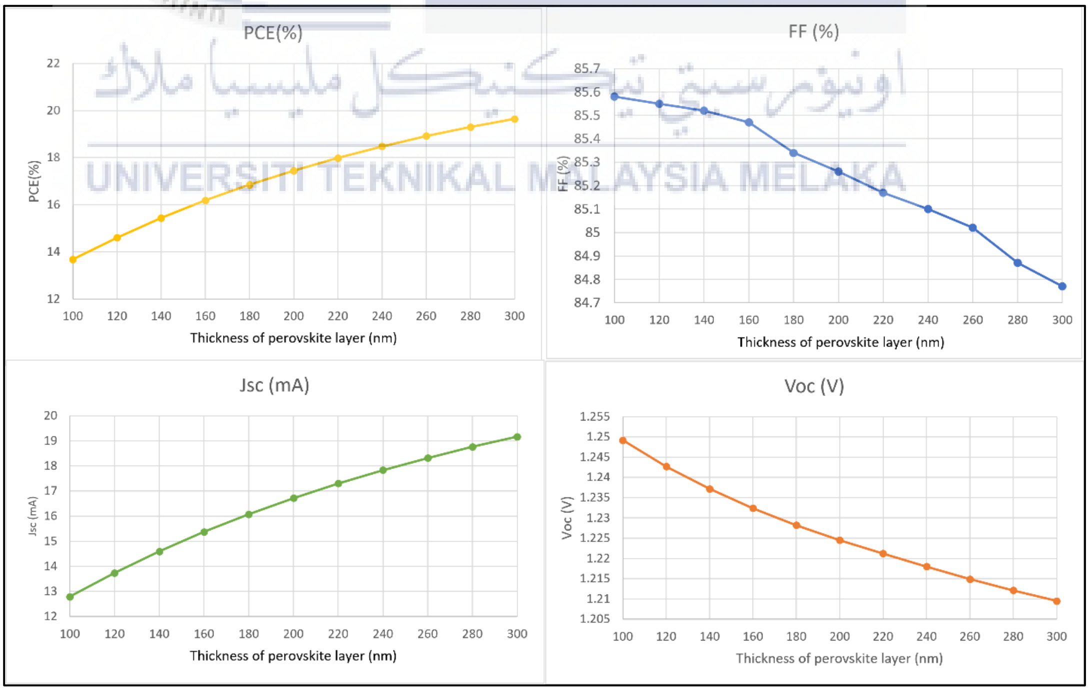

Figure 4.2: Graph For PCE, FF, Jsc And Voc With Thickness of Perovskite Layer From range 100 nm to 300 nm

Based on Figure 4.2, it can be observed that as the thickness of perovskite varied from 100 nm to 300nm, there is a clear increasing trend in power conversion efficiency (PCE). The PCE value rises from 13.68% at 100 nm to 19.65% at 300 nm. This suggests that, within the studied range, a thicker perovskite layer contributes positively to the overall efficiency of the solar cell. This may be due to improved light absorption and charge carrier generation with increased perovskite thickness. For Fill Factor (FF), the trend of fill factor value decrease as the perovskite layer thickness value increases, which is the FF value starting at 85.58% at 100 nm and it decreases to 84.77% at 300 nm. This indicates that the increase in perovskite thickness might lead to challenges in maintaining efficient charge transport. While for short circuit current (Jsc), the value increases as long the perovskite layer thickness value increases. This suggests that the higher thickness allows for more effective absorption of photons, leading to an increased generation of current. In addition, the rise in Jsc contributes positively to the overall performance of the solar cell. Lastly, for open-circuit voltage (Voc) shows a slight decrease as the perovskite layer thickness increases. This reduction may be attributed to increased charge recombination or other factors associated with thicker perovskite layers.

4.3 Analysis of Capture Cross Sections Electrons on Perovskite Layer.

Analyzed the value of capture cross-sections of electrons because it affects PSC efficiency. Firstly, the value of capture cross-sections of electrons has been varied from 1×10^{-19} cm² to 1×10^{-7} cm². Table 4.3 shows a set of parameter values for four parameters which is PCE, FF, J_{sc} and V_{oc}. The graph of a varied value of capture cross-sections of electrons is illustrated in Figure 4.3. The capture cross-sections represent the probability of the trap capturing the free carrier. As shown in Table 4.3 and Figure 4.3, if the value of capture cross-sections of electrons less than 1×10^{-10}cm² is almost constant. Whereas, if the value of capture cross-section increases from 1×10^{-19} cm² and above, the PSC shows a clear decreasing trend with increasing capture cross section.

Table 4.3: The Efficiency of PSC at Different Value of Capture Cross Sections of Electrons

Indicator for CCSE in graph	Capture cross section electrons (cm²)	PCE (%)
1	1×10^{-19}	25.01
2	1×10^{-18}	24.4
3	1×10^{-17}	22.6
4	1×10^{-16}	20.76
5	1×10^{-15}	19.65
6	1×10^{-14}	18.8
7	1×10^{-13}	17.88
8	1×10^{-12}	16.74
9	1×10^{-11}	15.7
10	1×10^{-10}	15.27
11	1×10^{-9}	15.19
12	1×10^{-8}	15.18
13	1×10^{-7}	15.18

As the cross section goes from 1×10^{-19} cm² to 1×10^{-7} cm², PCE drops from 25.01% to 15.18%. Higher capture cross sections are likely leading to more recombination events and reducing the efficiency of the solar cell. From Figure 4.3, Fill Factor (FF) also exhibits a consistent decrease which is 86.54% to 71.47% as the capture cross section increases. This suggests that higher capture cross sections result in reduced charge carrier mobility and increased resistive losses within the solar cell, impacting FF negatively. The degradation of J_{sc} from 19.166 mA to 18.243 mA has been observe when capture cross-section was varied from 1×10^{-19} cm² to 1×10^{-7} cm². Additionally, it was noted that the Voc decreased slightly from 1.508 V to 1.164

V when the capture cross-section area was raised. For instance, the lower the capture cross-sections area for electrons, it will increase the carrier's lifetime and eventually increase the efficiency [22]. The lifetime of carriers is determined by the trap density and carriers capture cross-section. An increase in the cross-section, the carrier lifetime decreases. This is because dimension of defect trap increases leads to significantly decrease the solar cells performance [23].

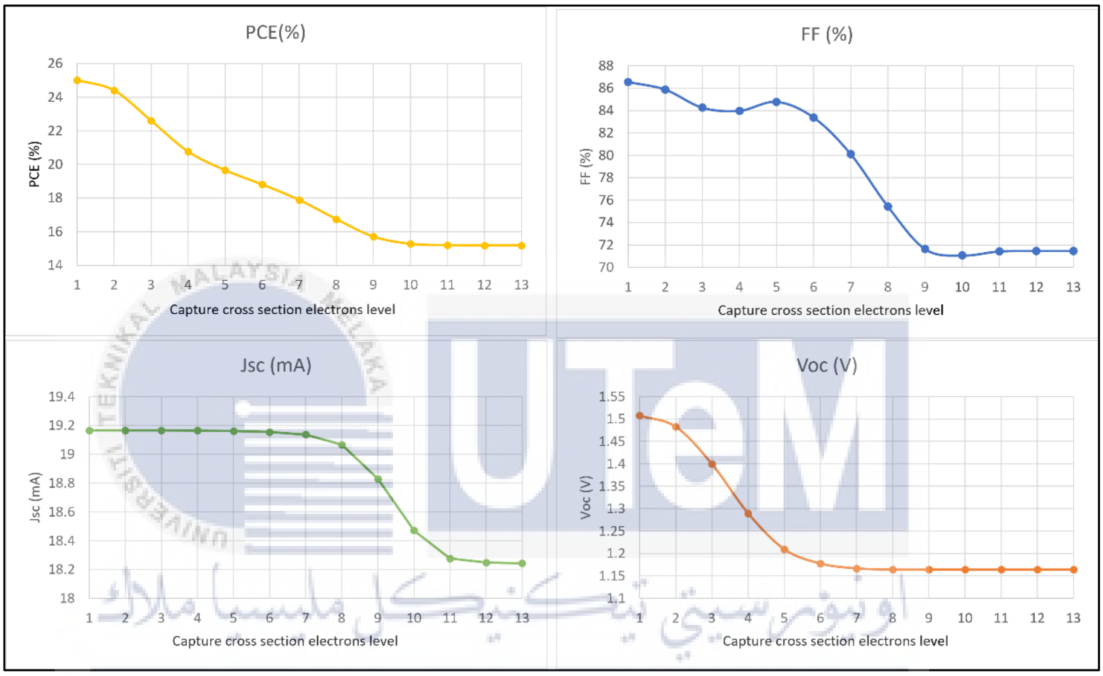

Figure 4.3: The Variation of Capture Cross-Sections of Electrons on PCE, FF, J_{sc} and V_{oc}

4.4 Analysis of capture cross-sections holes on perovskite layer.

Analyzed the value of capture cross-sections of holes because it affects PSC efficiency. Firstly, the value of capture cross-sections of electrons has been varied from 1×10^{-19} cm² to 1×10^{-7} cm² as shown at Table 4.4. The graph of a varied value of capture cross-sections of holes with four parameters which is PCE, FF, J_{sc} and V_{oc} is illustrated in Figure 4.4.

Table 4.4: The Efficiency of PSC at Different Value of Capture Cross Sections of Holes

Indicator for CCSE in graph	Capture cross section holes (cm^2)	PCE (%)
1	1×10^{-19}	25.02
2	1×10^{-18}	24.52
3	1×10^{-17}	22.88
4	1×10^{-16}	20.8
5	1×10^{-15}	19.65
6	1×10^{-14}	18.68
7	1×10^{-13}	17.25
8	1×10^{-12}	14.68
9	1×10^{-11}	11.35
10	1×10^{-10}	9.77
11	1×10^{-9}	9.52
12	1×10^{-8}	9.47
13	1×10^{-7}	9.47

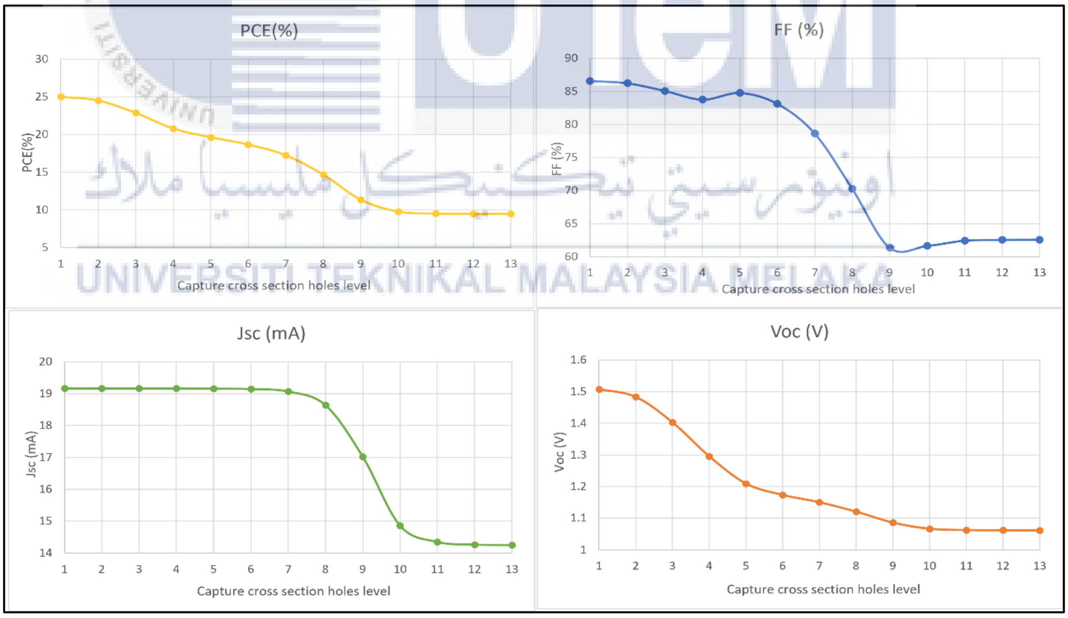

Figure 4.4: The Variation of Capture Cross-Sections of Holes on PCE, FF, J_{sc}

The capture cross section for holes represents the likelihood of holes being captured in the perovskite layer. According to Table 4.4, as the capture cross section increases, the performance of the solar cell generally decreases. Form the Figure 4.4 above, there are graph for variation of capture cross-sections of holes on PCE, FF, **Jsc** in PSC performance. For power conversion efficiency (PCE), PCE demonstrates a consistent decline with increasing capture cross section for holes. From 25.02% at 1×10^{-19} cm² to 9.47% at 1×10^{-7} cm², the trend indicates that higher capture cross sections negatively impact the efficiency of the solar cell. While Fill Factor (FF) also shows a decreasing trend as the capture cross section for holes increases.

This implies that higher capture cross sections contribute to reduced charge carrier mobility and increased resistive losses within the perovskite layer, leading to lower FF values. For Short-Circuit Current (Jsc), Short-Circuit Current (Jsc) follows a decreasing trend with higher capture cross sections for holes. This suggests that as more holes are captured, fewer contribute to the overall current generated by the solar cell, resulting in a reduction in Jsc. Lastly, Open-Circuit Voltage (Voc) experiences a decline with increasing capture cross section for holes. This may be attributed to increased charge recombination, affecting the ability to maintain a high voltage under open-circuit conditions.

4.5 Analysis of defect density of perovskite layer.

Analyzed the defect density of perovskite layer because it affects PSC efficiency Form table 4.5, the defect density of perovskite layer varied from 1×10^{7} cm^{-2} to 1×10^{19} cm^{-2} and the defect density parameters are illustrated in the graph in Figure 4.5. From Figure 4.5, PCE ranges from 25.1% at lower defect densities to 0.1% at higher defect densities. Higher defect densities lead to significant decrease in PCE, indicating that defects in the perovskite layer adversely impact the efficiency of the solar cell. For fill factor (FF), FF follows a decreasing trend from 86.63% to 32.44% as defect density increases. The increased defect density results in reduced charge carrier mobility and increased resistive losses, leading to a decrease in fill factor. Next, for short circuit current (Jsc), it maintains a relatively consistent value, with a slight decrease at higher defect densities which start at 1×10^{16}.

Table 4.5: The Range defect density of Perovskite Layer

Indicator for defect density in graph	Total defect density ($1/\ cm^2$)	PCE (%)
1	1×10^{7}	25.1
2	1×10^{8}	25.1
3	1×10^{9}	25.09
4	1×10^{10}	25.09
5	1×10^{11}	25.06
6	1×10^{12}	24.77
7	1×10^{13}	23.44
8	1×10^{14}	19.65
9	1×10^{15}	17.61
10	1×10^{16}	14.06
11	1×10^{17}	6.72
12	1×10^{18}	1.03
13	1×10^{19}	0.1

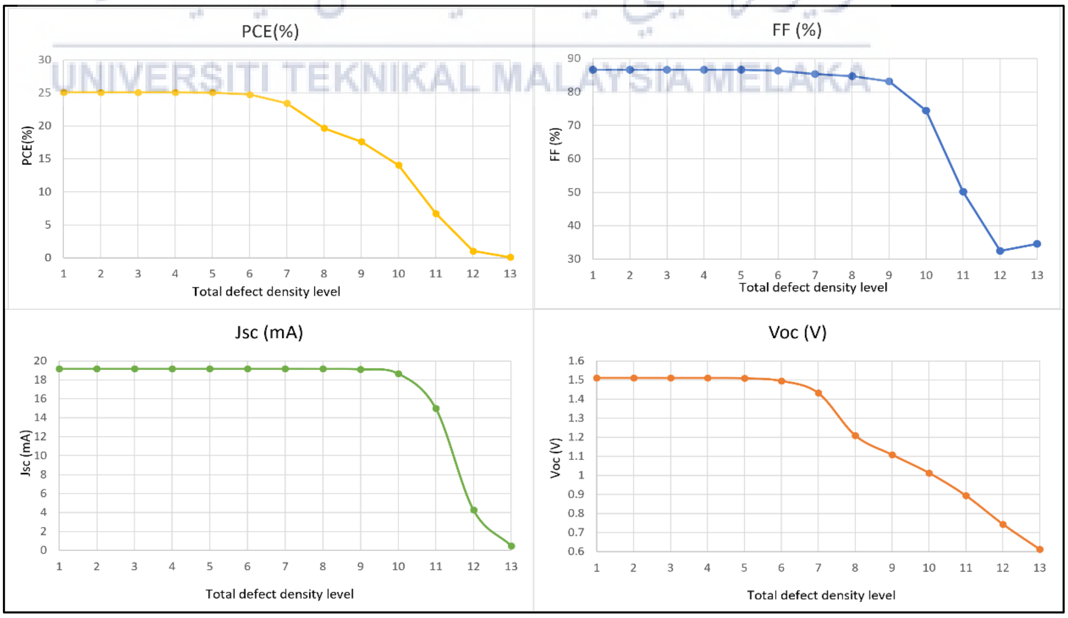

Figure 4.5: The Variation of Defect Density of Perovskite on PCE, FF, Jsc and Voc

Lastly, for Open-Circuit Voltage (Voc), the Voc decreases from 1.5114 V to 0.6121 V with increasing defect density. Higher defect densities result in a significant reduction in Voc, indicating increased charge recombination and a compromised ability to maintain a high voltage under open circuit conditions. In summary, the overall decrease in PCE suggests that other factors, such as decreased FF and Voc, contribute to the efficiency loss at higher defect densities of perovskite layer.

4.6 Optimization using Taguchi Method

The cell parameters were analyzed using Taguchi method L_9 (3^4) which has 9 experiments were used. The experimental layout for the four process parameters using L_9 orthogonal array is shown in Table 4.6.

Table 4.6: Experimental Layout using L_9 (3^4) Orthogonal Array

Expt. No.	Control Factors				S/N Ratio (dB)
	A Thickness of perovskite layer (nm)	B Capture cross section of electrons	C Capture cross-section of holes	D Defect density of Perovskite	
1	1	1	1	1	η_1
2	1	2	2	2	η_2
3	1	3	3	3	η_3
4	2	1	2	3	η_4
5	2	2	3	1	η_5
6	2	3	1	2	η_6
7	3	1	3	2	η_7
8	3	2	1	3	η_8
9	3	3	2	1	η_9

In this section, the PCE, FF, J_{sc} and V_{oc} were analyzed. The process parameter settings were found using the Taguchi experimental design method. The control variables are important process parameters which is the Thickness of perovskite layer, capture cross section of holes and the other two is capture cross-sections of electrons and defect density of Perovskite. Three levels of treatment are applied to the four control factors. Because the effect of these parameters on the performance requirements may differ, three levels have been chosen.

Meanwhile, the two noise factors are thickness of GO and Donor Density of GO. Each of the noise factors was varied for 2 levels to obtain four reading of PCE, FF, J_{sc} and V_{oc} of experiment. The signal-to-noise ratio (SNR) is determined to study the elements that influence the response and interpret the measured study results. To enable a "bigger is better" response and provide high results, the best value for each selected experience was determined by comparing the signal-to-noise ratio (SNR) [24]. Therefore, the process parameter fluctuation can be improved by selecting the right testing condition (noise factor settings) during Robust Design experiments.

Table 4.7 and Table 4.8 list the values of the process parameter and noise factor at various levels respectively. Nine different experiments using the design parameter combinations in the provided orthogonal array table, on the thickness of perovskite layer, capture cross-section holes, capture cross-section electrons defect density of perovskite layer, were performed. For each set of parameter combinations, four experiments were simulated. The next stage is to identify which control parameters can have an impact on a device characteristic after the response for PCE data using the L_9 array has been completed. The most effective combinations were quickly identified using the signal-to-noise. (S/N) ratio. PCE of IPSC devices is one of the larger-the-best quality parameters in this study. This signal-to-noise (S/N) ratio was used as reference to determine the value of PCE after using L_9 array predict or not.

Table 4.7: Process Parameters and The Levels

CONTROL FACTORS \ LEVELS	LEVELS		
	1	2	3
Thickness of perovskite layer (A)	100	200	100
Capture cross section of electrons (B)	1×10^{-17}	1×10^{-16}	1×10^{-15}
Capture cross section of holes (C)	1×10^{-17}	1×10^{-16}	1×10^{-15}
Defect density of perovskite layer (D)	1×10^{12}	1×10^{13}	1×10^{14}

Table 4.8: Noise Factors and The Levels

NOISE FACTORS \ LEVELS	Noise Level 1	Noise Level 2	Number of Levels
GO Thickness (μm) (M)	0.05	0.15	2
GO Donor Density (cm-3) (N)	5×10^{18}	5×10^{17}	2

4.6 Optimization of PCE in PSC devices

Table 4.9 illustrates the PCE findings for the PSC device employing the L_9 orthogonal array. The next stage is to establish the required values for a few parameters, including the thickness of perovskite layer, capture cross-section holes, capture cross-section electrons defect density of perovskite layer that had an impact on a device. Based on Table 4.10, it shows the value of S/N ratio the quality characteristics is larger-the-better. By using Eqn. 3.6, the η for each experiment was calculated.

Orthogonal is used as the experimental design, the effect of each process parameter on the S/N Ratio at various levels may be distinguished. Table 4.10 summarizes the S/N ratio for each level of the process parameters. In addition, the overall mean S/N ratio for the nine studies is computed and presented in Table 4.10. Table 4.11 shows the result of ANOVA for PCE in PSC devices. Generally, the PCE quality characteristic improves as the S/N ratio increases. The closer the quality characteristic value is to the target, the higher the quality of the product [32].

Table 4.9: PCE Values for PSC Devices

Expt. No.	Repetitions or Measurements for each expt.			
	1	2	3	4
1	16.52	16.46	16.93	16.87
2	15.96	15.91	16.36	16.31
3	13.68	13.63	14.02	13.97
4	20.11	20.09	20.29	20.27
5	21.42	21.38	21.60	21.56
6	21.44	21.39	21.62	21.57
7	24.44	24.43	24.52	24.51
8	22.95	22.93	23.03	23.01
9	24.56	24.50	24.64	24.59

Table 4.10: S/N respond for the PCE

Mean Sum of Squares of reciprocals	S/N Ratio (Larger-the-Better)
3.59×10^{-3}	27.39
3.84×10^{-3}	25.76
5.23×10^{-3}	24.63
2.45×10^{-3}	26.40
2.17×10^{-3}	26.36
2.16×10^{-3}	24.87
1.67×10^{-3}	26.61
1.89×10^{-3}	25.56
1.66×10^{-3}	25.42

For PCE, control factors capture cross section holes (Factor B), capture cross section electrons (Factor C) and defect density of perovskite layer (Factor D) were found level 1 as dominant factor because it has maximum S/N Ratio (η), while thickness of perovskite layer (Factor A) was found level 3 as dominant factor because it has maximum S/N Ratio (η). In addition, control factor A has the most significant effect on PCE of PSC device because the effect of that factor is high when compare to other control factors which is 92%. Where the effect of both control factors B and C are only 1%, while for control factor D is 6% effect.

Table 4.11: The Values Obtained of ANOVA for PCE in PSC Devices

CONTROL FACTORS	LEVEL			Degrees of Freedom	Sum of Squares	Mean Square	Factor Effect (%)	Empty or pooled F=<1.5
	1	2	3					
Thickness of perovskite layer (A)	23.80	26.47	**27.60**	2	23	11	92	no
Capture cross section holes (B)	**26.11**	26.01	25.76	2	0	0	1	pooled
Capture cross section electrons (C)	**26.11**	26.02	25.74	2	0	0	1	pooled
Defect density of perovskite layer (D)	**26.30**	26.19	25.38	2	2	1	6	no

Figure 4.6 shown the S/N Ratio (Larger-the-best) graphs where he dashed line is the value of the total mean of the S/N ratio and the other is factor effects. This graph is illustrated from Table 4.11 which is that the higher the level of the control factor is the dominant factor because it has the maximum S/N Ratio (η). Table 4.12 shows that the optimum levels have been selected due to the higher S/N ratio. The final step, following the selection of the ideal level of process parameters, is to predict and validate the improvement of the performance characteristic using the optimal level of process parameters. The S/N ratio of optimum level for the process parameters is 27.98dB which is predict to the performance characteristics.

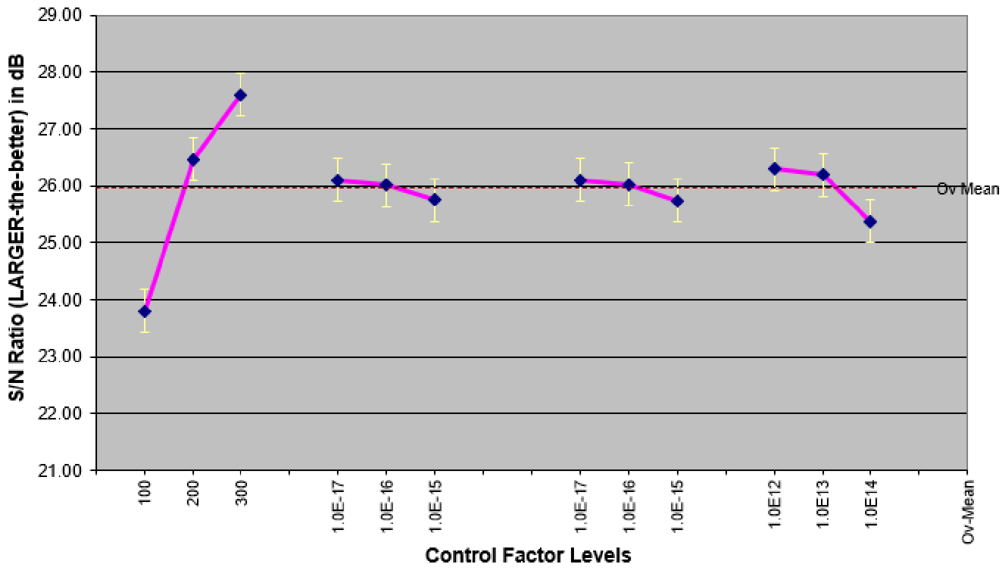

Figure 4.6: S/N Graph of PCE for PSC

Table 4.12: Predict S/N Ratio of PCE in PSC Devices

CONTROL FACTORS	LEVELS 1	LEVELS 2	LEVELS 3	Optimum level	Level Name	Factor Effect (%)	Dominant/ Significant/ Neutral
Thickness of erovskite layer(A)	100	200	100	3	300	96	Dominant
Capture cross section holes (B)	1×10^{-17}	1×10^{-16}	1×10^{-15}	1	-	1	Neutral
Capture cross section electrons (C)	1×10^{-17}	1×10^{-16}	1×10^{-15}	1	-	1	Neutral
Defect density of perovskite layer (D)	1×10^{12}	1×10^{13}	1×10^{14}	1	$1 \text{ x } 10^{12}$	6	Significant
S/N Ratio				27.9			
		28.49				27.31	

4.6 Optimization of FF in PSC devices

The results of FF in PSC device using L_9 orthogonal array is shown in Table 4.13. After nine experiments of L_9 array were performed, the calculated S/N ratio values using Eqn. 3.6 has been shown in Table 4.14. Based on Table 4.14, it shows the S/N ratio value for the quality characteristics larger-the-better.

Table 4.13: FF Values for PSC Devices

Expt. No.	Repetitions or Measurements for each expt.			
	1	2	3	4
1	86.65	86.48	86.69	86.51
2	86.04	85.92	86.08	85.95
3	85.58	85.54	85.66	85.57
4	85.01	84.95	85.02	84.98
5	86.25	86.17	86.25	86.17
6	86.40	86.28	86.40	86.28
7	85.97	86.02	85.97	86.02
8	85.13	85.12	85.14	85.12
9	86.26	86.16	86.27	86.16

Table 4.14: S/N Respond for the FF

Mean Sum of Squares of reciprocals	S/N Ratio (Larger-the-Better)
1.33×10^{-4}	38.75
1.35×10^{-4}	38.69
1.37×10^{-4}	38.65
1.38×10^{-4}	38.59
1.35×10^{-4}	38.71
1.34×10^{-4}	38.72
1.35×10^{-4}	38.69
1.38×10^{-4}	38.60
1.35×10^{-4}	38.71

Table 4.15 shows the result of ANOVA for FF in PSC devices. Generally, for FF in IPSC devices, the defect density of perovskite layer (Control Factor B – 85%) was determined to be the main factor influencing fill factor, FF. This is because control factors B have the highest percent effect compared to other control factors which are

for 3 control factors only have effect 5% for each factor. The analysis of average performance indicates the optimum condition to be $A_1B_3C_1D_1$.

Table 4.15: The Values Obtained of ANOVA for FF in PSC Devices

CONTROL FACTORS	LEVEL			Degrees of Freedom	Sum of Squares	Mean Square	Factor Effect (%)	Empty or pooled F=<1.5
	1	2	3					
Thickness of perovskite layer (A)	**38.70**	38.67	38.67	2	0	0	5	no
Capture cross section holes (B)	38.68	38.67	**38.69**	2	0	0	5	pooled
Capture cross section electrons (C)	**38.69**	38.66	38.68	2	0	0	5	no
Defect density of perovskite layer (D)	**38.72**	38.70	38.61	2	0	0	85	no

Figure 4.7 shows the S/N Ratio (Larger-the-best) graphs where each control factors with the higher S/N Ratio (η) is the dominant factor. The dashed line the value of the total mean of the S/N ratio and the straight line is factor effects.

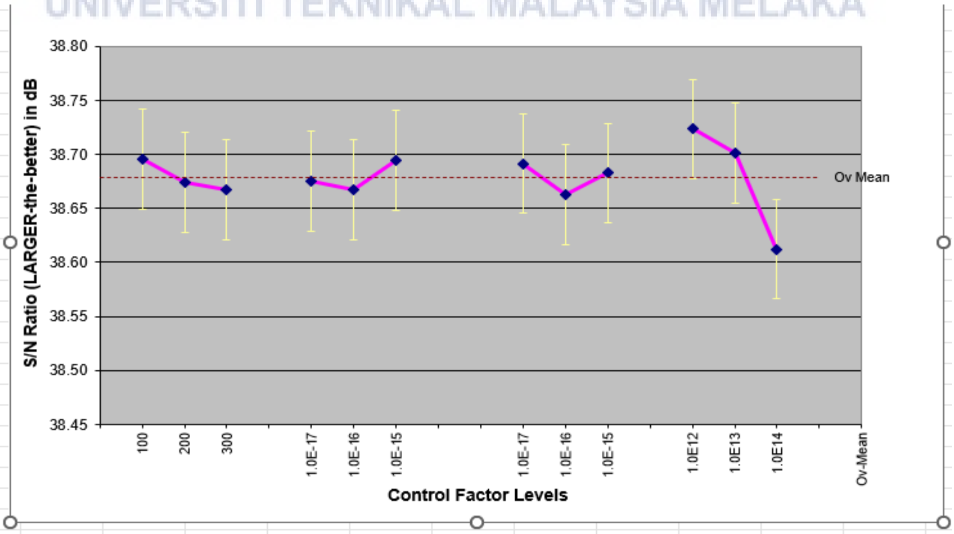

Figure 4.7: S/N Graph of FF for PSC Devices

The level that was chosen because of the increased S/N ratio is shown in Table 4.16. The final stage is to predict and confirm the increase in the performance characteristic using the optimal level of the process parameters once the optimal level of the process parameters has been chosen. The optimal S/N ratio for the process parameters is 38.75dB which is approximately to the predicted value.

Table 4.16: Predict S/N Ratio of FF in PSC Devices

CONTROL FACTORS	LEVELS 1	LEVELS 2	LEVELS 3	Optimum level	Level Name	Factor Effect (%)	Dominant/ Significant/ Neutral
Thickness of perovskite layer(A)	100	200	100	1	100	5	Neutral
Capture cross section holes (B)	1×10^{-17}	1×10^{-16}	1×10^{-15}	3	1×10^{-15}	5	Neutral
Capture cross section electrons (C)	1×10^{-17}	1×10^{-16}	1×10^{-15}	1	1×10^{-17}	5	Neutral
Defect density of perovskite layer (D)	1×10^{12}	1×10^{13}	1×10^{14}	1	1×10^{12}	85	Dominant
S/N Ratio				38.8			
		38.84				38.66	

4.6. Optimization of J_{sc} in PSC Devices

Table 4.17 displays the results of the J_{sc} in the PSC device utilizing the L_9 orthogonal array. After nine experiments from L_9 array have been completed, the next stage is to identify the required values for chosen parameters, including the thickness of perovskite layer, capture cross-section of electrons, capture cross-section of holes and defect density of perovskite layer, which had an effect on the device. According to Table 4.18, the higher the S/N ratio, the higher the quality characteristics. By using Eqn. 3.6, the η for each experiment was calculated. The orthogonal experimental design allows for the separation of the effects of each process parameter on the S/N Ratio at various levels.

Table 4.17: The Values of J_{sc} for PSC Devices

Expt. No.	Repetitions or Measurements for each expt.			
	1	2	3	4
1	12.793	12.792	13.092	13.092
2	12.793	12.792	13.092	13.092
3	12.793	12.792	13.092	13.091
4	16.718	16.718	16.854	16.854
5	16.718	16.718	16.854	16.854
6	16.718	16.718	16.854	16.854
7	19.166	19.166	19.229	19.229
8	19.166	19.166	19.228	19.22
9	19.166	19.1664	19.229	19.229

Table 4.18: S/N Respond for the J_{sc} of Nine Experiments

Mean Sum of Squares of reciprocals	S/N Ratio (Larger the Better)
5.97×10^{-3}	22.24
5.97×10^{-3}	22.24
5.97×10^{-3}	22.24
3.55×10^{-3}	24.50
3.55×10^{-3}	24.50
3.55×10^{-3}	24.50
2.71×10^{-3}	25.66
2.71×10^{-3}	25.66
2.71×10^{-3}	25.66

In Table 4.19 shows the result of ANOVA for Jsc in PSC devices, the most effective process parameters with respect to the performance of PSC devices are thickness of perovskite layer (Control Factor A – 100%). According to Table 4.19, thickness of perovskite layer was found to be the major factor affecting the performance of PSC compared to other control factors 0%. An effect control factors 0% that it does not affect the short-circuit current, J_{sc}. The analysis of average performance indicated that the optimal condition existed is $A_3B_1C_1D_1$.

Table 4.19: The Values Obtained of ANOVA for J_{sc} in PSC Devices

CONTROL FACTORS	LEVEL			Degrees of Freedom	Sum of Squares	Mean Square	Factor Effect (%)	Empty or pooled F=<1.5
	1	2	3					
Thickness of perovskite layer (A)	22.24	24.50	**25.66**	2	18	9	100	no
Capture cross section holes (B)	24.13	24.13	24.13	2	0	0	0	pooled
Capture cross section electrons (C)	24.13	24.13	24.13	2	0	0	0	no
Defect density of perovskite layer (D)	24.13	24.13	24.13	2	0	0	0	no

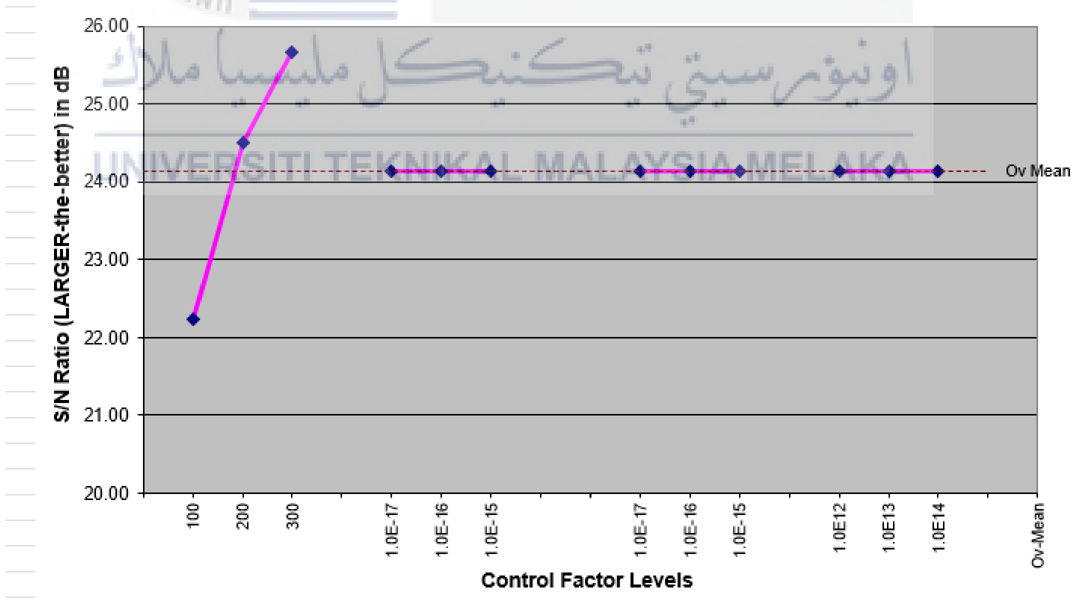

Figure 4.8: S/N Graph of J_{sc} for PSC Device

The S/N Ratio (Larger-the-Best) graphs are shown in Figure 4.8, with the factor effects represented by the straight line and the total mean of the S/N ratio represented by the dotted line. As depicted by this graph, which is taken from Table 4.19, the greater the level of the control factor, which has the highest S/N Ratio (η), the more dominant factor it is. For instance, thickness of perovskite layer (Control Factor A) has the highest S/N Ratio (η), compared to others control factors at same level of the total mean. From Table 4.20, for J_{sc} in PSC devices, thickness of perovskite layer (Control Factor A -100%) was defined as the major factor affecting the J_{sc} in PSC. The factor A effect was 100% compared to another factor effect which is 0% or neutral was found not significant to the short-circuit current, J_{sc}. The optimal S/N ratio for the process parameter, which predicts the performance characteristics, is 25.66dB.

Table 4.20: Predict S/N Ratio of J_{sc} in PSC Devices

<table>
<tr><th rowspan="2">CONTROL FACTORS</th><th colspan="3">LEVELS</th><th rowspan="2">Optimum level</th><th rowspan="2">Level Name</th><th rowspan="2">Factor Effect (%)</th><th rowspan="2">Dominant/ Significant/ Neutral</th></tr>
<tr><th>1</th><th>2</th><th>3</th></tr>
<tr><td>Thickness of perovskite layer(A)</td><td>100</td><td>200</td><td>100</td><td>3</td><td>100</td><td>100</td><td>Dominant</td></tr>
<tr><td>Capture cross section holes (B)</td><td>1×10^{-17}</td><td>1×10^{-16}</td><td>1×10^{-15}</td><td>1</td><td>1×10^{-17}</td><td>0</td><td>Neutral</td></tr>
<tr><td>Capture cross section electrons (C)</td><td>1×10^{-17}</td><td>1×10^{-16}</td><td>1×10^{-15}</td><td>1</td><td>1×10^{-17}</td><td>0</td><td>Neutral</td></tr>
<tr><td>Defect density of perovskite layer (D)</td><td>1×10^{12}</td><td>1×10^{13}</td><td>1×10^{14}</td><td>1</td><td>1×10^{12}</td><td>0</td><td>Neutral</td></tr>
<tr><td colspan="2" rowspan="2">S/N Ratio</td><td colspan="2"></td><td colspan="2">25.7</td><td colspan="2"></td></tr>
<tr><td colspan="2">25.72</td><td colspan="2"></td><td colspan="2">25.61</td></tr>
</table>

4.7. Optimization of V_{oc} in PSC Devices

The results of V_{oc} in PSC device using L_9 orthogonal array is depicted in Table 4.21. After nine experiments of L_9 array have been implemented, the value of S/N ratio have been calculated by using Equation (3.6) as shown in Table 4.22. Based on Table 4.22, it shows the value of S/N ratio the quality characteristics is larger-the-better. By using Eqn. 3.6, the η for each experiment was calculated.

Table 4.21: V_{oc} Values for PSC Devices

Expt. No.	Repetitions or Measurements for each expt.			
	1	2	3	4
1	1.4902	1.4880	1.4915	1.4894
2	1.4501	1.4479	1.4514	1.4492
3	1.2492	1.2456	1.2502	1.2467
4	1.4152	1.4149	1.4157	1.4153
5	1.4855	1.4839	1.4859	1.4843
6	1.4845	1.4827	1.4849	1.4831
7	1.4831	1.4817	1.4833	1.4819
8	1.4068	1.4055	1.4070	1.4057
9	1.4854	1.4838	1.4855	1.4840

Table 4.22: S/N Respond for the V_{oc} for Nine Experiments

Mean Sum of Squares of reciprocals	S/N Ratio (Larger the Better)
4.51×10^{-3}	3.46
4.76×10^{-3}	3.23
6.42×10^{-3}	1.92
4.99×10^{-3}	3.02
4.54×10^{-3}	3.43
4.54×10^{-3}	3.43
4.55×10^{-3}	3.42
5.06×10^{-3}	2.96
4.54×10^{-3}	3.43

In this experiment as mentioned, with using L_9 orthogonal array, it is possible to isolate the effect of each process parameter on the S/N ratio at various levels. As depicted in Table 4.23, the S/N ratio for each level of the process parameter is summarized. From table 4.23, for open-circuit voltage, V_{oc} in PSC devices, defect density of perovskite (Control Factor D – 60%) and thickness of perovskite layer (Control Factor A – 17%) were deemed to be the main influence on the V_{oc}.

Table 4.23: The Values Obtained of ANOVA for V_{oc} in PSC Devices

CONTROL FACTORS	LEVEL			Degrees of Freedom	Sum of Squares	Mean Square	Factor Effect (%)	Empty or pooled F=<1.5
	1	2	3					
Thickness of perovskite layer (A)	2.87	**3.29**	3.27	2	0	0	17	no
Capture cross section holes (B)	**3.30**	3.21	2.93	2	0	0	11	no
Capture cross section electrons (C)	**3.28**	3.22	2.93	2	0	0	11	no
Defect density of perovskite layer (D)	**3.44**	3.36	2.63	2	1	1	60	no

This is because control factors B and D have a high percent contribution compared to other factors. The percentage effects on S/N ratio of capture cross section holes and capture cross-section of electrons are 11% for both control factors. According to Table 4.23, defect density of perovskite layer was found to be major factor affecting the V_{oc} in PSC devices. The analysis of average performance indicated that the optimum condition is $A_2B_1C_1D_1$. Figure 4.9 shown the S/N Ratio (Larger-the-best) graphs in which the dashed line represents the total mean of the S/N ratio, and the other line is factor effects.

The higher the level of the control factor is the dominant factor due to the maximum of S/N Ratio (η). As depicted in Table 4.24 shows the level has been selected due to the higher S/N ratio. Once the optimal level of the process parameters has been chosen and proceed to the final step which is to predict and verify the S/N ratio optimum level of the process parameters. The value of S/N ratio optimum level of the process parameters is 3.54dB which is approximately to the predict value 3.80dB.

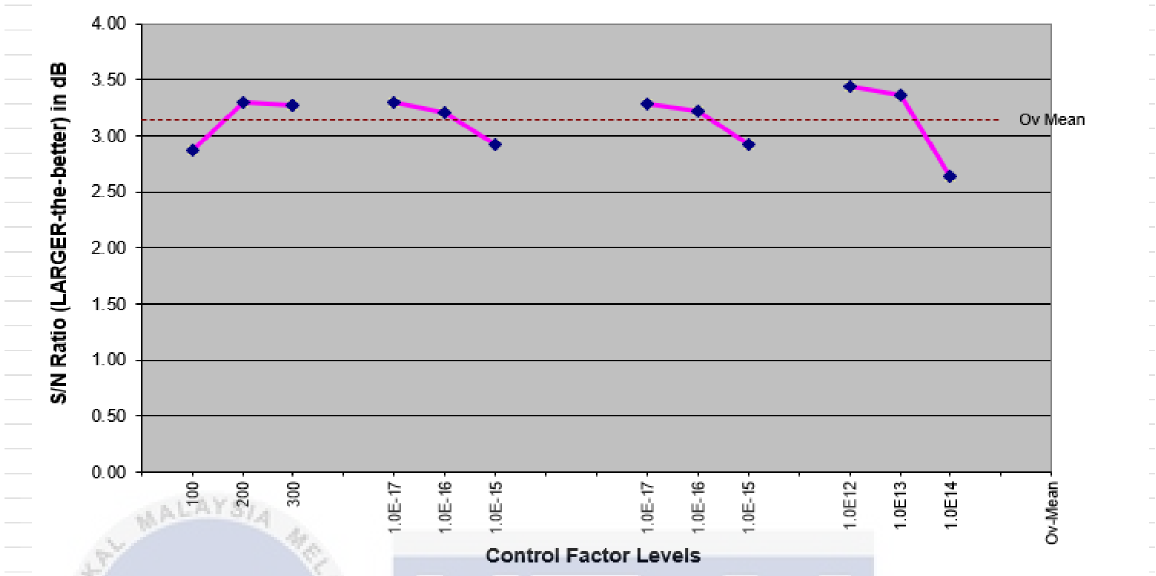

Figure 4.9: S/N Graph of V_{oc} for PSC Device

Table 4.24: Predict S/N Ratio of V_{oc} in PSC Devices

CONTROL FACTORS	LEVELS			Optimum level	Level Name	Factor Effect (%)	Dominant/ Significant/ Neutral
	1	2	3				
Thickness of perovskite layer(A)	100	200	100	2	200	17	Dominant
Capture cross section holes (B)	1×10^{-17}	1×10^{-16}	1×10^{-15}	1	1×10^{-17}	11	Significant
Capture cross section electrons (C)	1×10^{-17}	1×10^{-16}	1×10^{-15}	1	1×10^{-17}	11	Significant
Defect density of perovskite layer (D)	1×10^{12}	1×10^{13}	1×10^{14}	1	1×10^{12}	60	Dominant
S/N Ratio				3.9			
		3.97				3.8	

4.11 Multiple Optimization

Based on individual results from PCE, FF, J_{sc} and V_{oc}, the average performance analysis from each parameter was recorded. Each parameter shows the optimum level was chosen because of the higher S/N ratio. The percent effect on the S/N ratio indicates the dominant factor to the process parameter. From Table 4.25, it shows the multiple optimization results.

Table 4.25: The Level Obtained for Multiple Optimization in PSC Devices

Parameters	A	B	C	D	Value	S/N Ratio(dB)
PCE (%)	3 (92%)	1 (1%)	1 (1%)	1 (6%)	25.06	27.9
FF (%)	1 (5%)	3 (5%)	1 (5%)	**1 (85%)**	86.65	38.8
J_{sc} (mA/cm2)	**3 (100%)**	1 (0%)	1 (0%)	1 (0%)	19.17	25.7
V_{oc} (V)	2 (17%)	**1 (11%)**	**1 (11%)**	1 (60%)	1.5	3.9
Multiple Optimization	**3**	**1**	**1**	**1**		

Based on Table 4.25, the four control factors on each parameter namely PCE, FF, J_{sc} and V_{oc} show the percent effect on the S/N ratio. Firstly, the thickness of perovskite layer (Control Factor A) is selected level 3 (300nm) when it has more effect on J_{sc} due to the highest percent effect is 100% compared to other level only 0%. Next, for capture cross-section of holes (Factor B), level 1 (1 x 10^{-17} cm^{-3}) was chosen even though the percentage of effect is 11% but it is the highest percentage compared to other which.

Next, level 1 (1 x 10^{-17} cm^{-3}) is selected for capture cross-section of electrons (Factor C) because it has the highest percentage which is 11% from the other level. Lastly, the defect density of perovskites layer (Control Factor D), level 1 is the highest percent effect which is 85% compared to other levels. So, for defect density of perovskite layer level 1 (1 x 10^{12} cm^{-3}) was chosen. From Table 4.26, it shows each parameter that has been used before and after optimization. The perovskite layer thickness value after optimization is 300 nm which is the same as before optimization, Next. The cross-sectional capture of electrons and holes has changes 1×10^{-15} to 1×10^{-19} cm^2 after optimization that is commonly used from previous research. Lastly, to obtain a higher PCE in PSC devices above 25%, the perovskite defect density value should be considered.

Table 4.26: Parameter Before and After Optimization

Parameters	Initial PSCs	Optimized PSCs
Thickness of perovskite layer (nm)	300	300
Capture cross section electrons (cm^2)	1×10^{-15}	1×10^{-19}
Capture cross section electrons (cm^2)	1×10^{-15}	1×10^{-19}
Defect Density of perovskite layer cm^{-3}	1×10^{-14}	1×10^{-12}

Table 4.27: The Level Obtained for Multiple Optimization in PSC Devices

Parameters	Before Optimization	After Optimization		Previous Journal [6,12]
		Individual	Multiple	
PCE (%)	19.65	25.06	25.06	16.03
FF (%)	84.77	86.65	86.61	82.8
J_{sc} (mA/cm2)	19.16	19.17	19.17	21.73
V_{oc} (V)	1.21	1.50	1.51	0.89

Based on Table 4.26 and Figure 4.10, for power conversion efficiency (PCE), before Optimization, the initial PCE was 19.65%, indicating the efficiency of the solar cell before any optimization efforts. After optimization efforts focused on individual parameters, the PCE increased to 25.06%, showing a substantial. The PCE remains at 25.06%, indicating that the multiple parameter optimization strategy has achieved the same level of improvement as the individual optimization.

Besides, for fill factor (FF) before optimization, FF was 84.77% before any optimization. Following individual parameter optimization, the FF increased to 86.65%, highlighting enhanced charge carrier mobility and reduced losses. The FF slightly decreased to 86.61% after multiple parameter optimization. This could suggest a trade-off between certain parameters, emphasizing the complexity of optimizing multiple factors simultaneously.

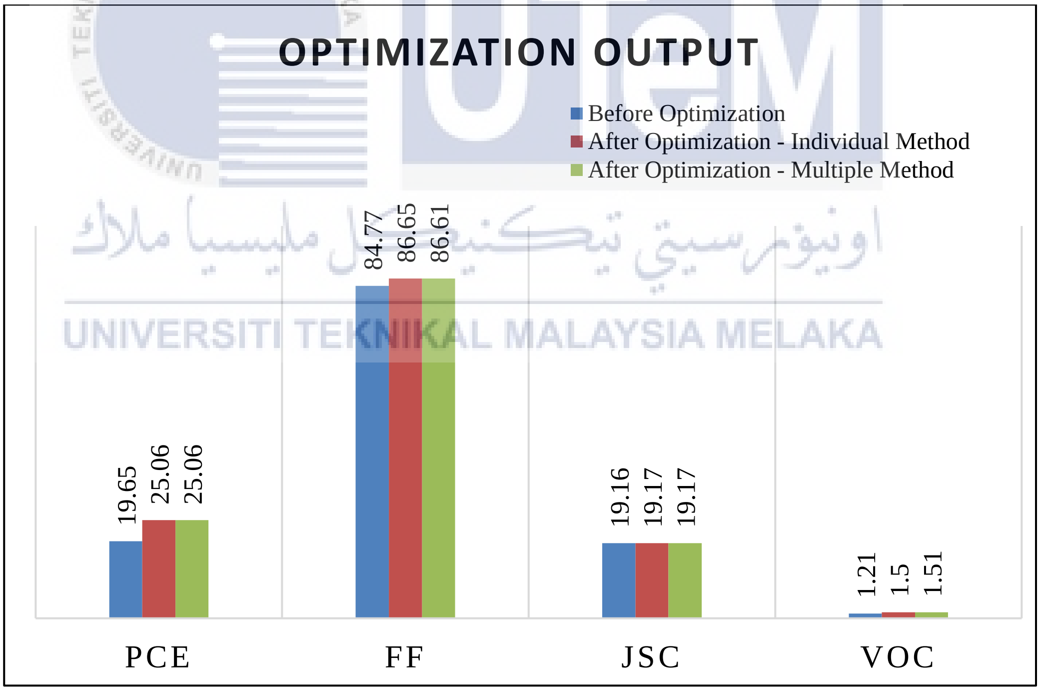

Figure 4.10: Comparison of Values Obtained Before and After Optimization

Next, short circuit current (Jsc), before Optimization, the initial Jsc was 19.16 mA/cm², reflecting the current generated when the solar cell operates under short-circuit conditions. After focusing on individual parameter optimization, Jsc increased to 19.17 mA/cm², indicating a subtle improvement in current generation. The Jsc remains at 19.17 mA/cm² after multiple parameter optimization, suggesting that the combined efforts maintained the current generation enhancement achieved through individual optimization. Lastly, for open circuit voltage (Voc), before Optimization, the initial Voc was 1.21 V, representing the maximum voltage across the solar cell under open-circuit conditions. After individual parameter optimization, Voc significantly increased to 1.50 V, indicating a successful enhancement in the voltage output. The Voc slightly increased to 1.51 V after multiple parameter optimization, reinforcing the positive impact of the combined optimization efforts.

In summary, the table illustrates the significant improvements achieved through optimization, both when focusing on individual parameters and when optimizing multiple parameters simultaneously. The balanced enhancement across PCE, FF, Jsc, and Voc demonstrates a comprehensive optimization strategy, resulting in an overall more efficient and effective solar cell from the previous research. Figure 4.11 shows the perovskite solar cell with graphene on ETL layer exhibits a stable and consistently high current density across various voltage levels for before and after optimization.

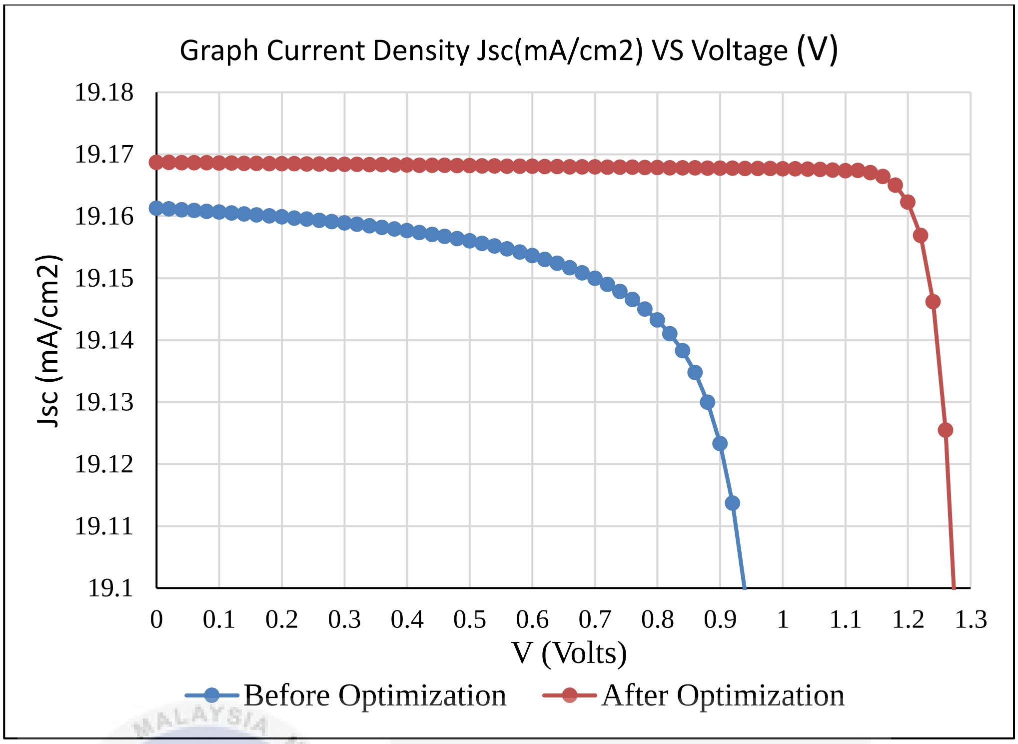

Figure 4.11: Comparison of Current Density and Voltage Obtained Before and After Optimization

Moreover, before optimization, the initial current density is around 19.16 A/m² and the stable open circuit voltage archived at around 0.3V. Meanwhile after optimization the initial current density is around 19.17 A/m² the stable open circuit voltage archived at around 1.1V. Thus, improvement for stability and promising performance of the perovskite solar cell has been proven by optimization using Taguchi method.

CHAPTER 5

CONCLUSION AND FUTURE WORKS

This chapter will discuss the overall conclusion by providing an overall summary of the project. Future works also will be suggested.

5.1 Conclusion

PSC is a type of perovskite solar cells having n-i-p (regular) and p-i-n (inverted). The placement of HTL and ETL is what differentiates these two topologies. For the perovskite solar cells with regular structure (PSC) the ETL layer is placed on bottom of TCO (transparent conducting oxide) substrate. By employing GO as ETL in PSC, the performance of PSC is encouraging as GO offers high charge mobility, reliability, low processing cost, large-scale production possibilities, and good dispersibility in a variety of solvents. Graphene oxide (GO) has gained attention as a potential electron transport layer (ETL) material in perovskite solar cells due to its unique properties.

Graphene oxide exhibits high electron mobility, allowing for efficient transport of electrons through the ETL.

This can contribute to improved charge extraction and reduced recombination losses in perovskite solar cells. The properties of graphene oxide can be easily tuned by controlling the degree of oxidation and functionalization. This tunability allows for optimization of the ETL to match the specific requirements of the perovskite solar cell. The main objective of this project, which is to simulate GO as ETL on a solar cell using SCAPS-1D simulation software, was succeeded. The simulation was implemented by employing a complete simulated device structure composed of FTO/GO/$CH_3NH_3PbI_3$/Cu_2O.

Besides, the analysis of this project which is to optimize GO as ETL also was successfully performed. Several key parameters of ETL have been analyzed to obtain the optimum performance. The simulation results showed that GO as ETL in PSC has produced an efficiency 19.65% compared to previous researcher of perovskite solar cell (PSC) containing graphene as ETL has achieved an optimal PCE of 16.03% using SCAPS-1D simulation. In addition, after optimization using Taguchi Method L_9 OA the efficiency increased to 25.06 %. This shows that the optimum solution in achieving the desired efficiency in PSC devices was successfully predicted by using Taguchi Method. Overall, the project was a success. Efficiency can be improved by using GO as ETL in PSC devices and optimizing it using Taguchi Method.

In addition, Graphene oxide possesses excellent mechanical strength, providing stability to the ETL layer. This can be advantageous for the long-term durability of the solar cell. Moreover, high fill factor of a solar cell is important because it is an indicator of the cell's overall efficiency. Next, the higher fill factor means that more of the area of the cell can capture and convert sunlight into electrical energy, allowing the cell to generate a higher output power. In additional, the short circuit current of a solar cell is important because it determines how much power the solar cell can produce. Thus, the higher the short circuit current, the more power the solar cell can produce for solar cells to be effective. This ensures that the solar cells can capture and store as much energy from the sun as possible. Lastly, the open voltage of a solar cell must be as high as possible because it directly affects the efficiency of the cell it is because the higher open voltage allows more of the solar energy to be converted into usable electrical power.

5.2 Future works

In the future, the optimization results can be used as a guide in the fabrication process for PSC employing GO as electron transport layer. The performance of GO as ETL in PSC device can be improved by do analysis on defect density of perovskite layer. Toxicity and environmental impact, perovskite solar cells often contain lead, which raises concerns about their potential environmental impact. Researchers are actively investigating lead-free alternatives and environmentally friendly fabrication processes to address these concerns and ensure the sustainability of perovskite technology. In addition, large area, and flexible devices. Perovskite solar cells can be fabricated on flexible substrates, enabling the possibility of lightweight, flexible, and even transparent solar panels.

Research efforts are focused on improving the mechanical stability and efficiency of large-area and flexible perovskite solar cells for various applications including wearable electronics, building-integrated photovoltaics (BIPV) and portable power generation. Moreover, in terms of efficiency improvement, although perovskite solar cells have achieved high power conversion efficiencies (PCEs) exceeding 25%, there is still room for improvement. Scientists and researchers are exploring novel materials, engineering techniques and device architectures to boost efficiency further and overcome issues like charge recombination and light absorption limitations. Lastly, tandem, and multi-junction devices. Perovskite solar cells can be combined with other solar cell technologies, such as silicon or thin-film solar cells, to create tandem or multi-junction devices. These configurations have the potential to achieve even higher efficiencies by utilizing a broader spectrum of sunlight.

REFERENCES

[1] Wang, L., Chang, B., Li, H., Wu, Y., Liu, Z., Pan, L., & Yin, modulation and organic spacerconstruction for stable perovskite solar cells." 2022 Energy &Environmental Science, 15(11), 4470–4510.

[2] Shin, S. J., Alosaimi, G., Choi, M. J. et al., "Strategic Approach for Frustrating Charge Recombination of Perovskite Solar Cells in LowIntensity Indoor Light: Insertion of Polar Small Molecules at the Interface of the Electron Transport Layer." 2022 ACS Applied Energy Materials, 5(11), 13234–13242.

[3] Steele, J et al., " An embedded interfacial network stabilizes inorganic CsPbI3 perovskite thin films." 2022 Nature Communications, 13(1), 7513.

[4] Yamada, Y., & Kanemitsu, Y., " Electron-phonon interactions in halide perovskites." 2022 NPG Asia Materials, 14(1), 48.

[5] Lee, M et al., "Enhanced Hole ‐ Carrier Selectivity in Wide Bandgap Halide Perovskite Photovoltaic Devices for Indoor Internet of Things Applications. " 2021 Advanced Functional Materials, 31(16), 2008908.

[6] Abadi, N. M. S., Banihashemi,"Simulation and Analysis of a Perovskite Solar Cell with (FAPbI 3) 0.85 (MAPbBr 3) 0.15 as Absorber Layer." 2019 27th Iranian Conference on Electrical Engineering (ICEE), 173–177.

[7] M. Salah et al., "A Comparative Study of Different ETMs in Perovskite Solar Cell with Inorganic Copper Iodide as HTM." 2018 DOI:10.1016/j.ijleo.2018.10.052

[8] Kwadwo M.-Darkwa, R. Namoe Tabi, P. K. Kahol and R. K. Gupta, "Graphene for Flexible Photovoltaic Devices." 2019 Journal of Solar Energy Research Updates.

[9] Aniseh Kafi, M. Hossein Zandi & Nima E. Gorji, "Simulation analysis of graphene contacted perovskite solar cells using SCAPS-1D." 2019 Volume 51, article number 91

[10] K. Mahmood, S. Sarwarb and M. T. Mehranb, "Current status of electron transport layers in perovskite solar cells: materials and properties." 2017 RSC Adv., 2017, 7, 17044

[11] A. Benami, L. Et-taya, T. Ouslimane and A. Sohani, "Comparison of the Effects of ZnO and TiO2 on the Performance of Perovskite Solar Cells via SCAPS-1D Software Package." 2022 Journal of Nano- and Electronic Physics. Materials & Design Volume 211

[12] Khairil Ezwan Kaharudin, Fauziyah Salehuddin, "Predictive Modeling Of Mixed Of Halide Perovskite Using Hybrid L27 OA Taguchi-Based GA-MLR-GA Appoach." 2021 Jurnal Teknologi

[13] R. babu, G. Lingamallu, "Recent Advances in Halide-based Perovskite Crystals and Its Optoelectronic Applications." 2018 Crystal Growth & Design 18(4) DOI:10.1021/acs.cgd.7b01767

[14] Babu, R.; Giribabu, L.; Singh, S.P. Recent advances in halide-based perovskite crystals and their optoelectronic applications. Cry. Growth Des. 2018, 18, 2645–2664.

[15] González-Carrero, S.; Galian, R.E.; Pérez-Prieto, J. Organometal halide perovskites: Bulk low-dimension materials and nanoparticles. Part. Part. Syst. Charact. 2015, 32, 709–720.

[16] Susrutha, B.; Giribabu, L.; Singh, S.P. Recent advances in flexible perovskite solar cells. Chem. Commun. 2015, 51, 14696–14707.

[17] "Miyasaka, T. Perovskite photovoltaics: Rare functions of organo lead halide in solar cells and optoelectronic devices. Chem. Lett. 2015, 44, 720–729.

[18] K. S. Srivishnu,P. R. Markapudi, ea al., "Semitransparent Perovskite Solar Cells for Building Integrated Photovoltaics: Recent Advances." 2023 Energies, 16(2)

[19] Gagandeep, M. Singh; R. Kumar, "Simulation of perovskite solar cell with graphene as hole transporting material" 2019 RESEARCH ARTICLE AIP Conf. Proc. 2115, 030548

[20] M. Gholipoor, N. Solhtalab, M. Hosein Mohammadi, "High-performance parallel tandem MoTe2/perovskite solar cell based on reduced graphene oxide as hole transport layer." 2022 Scientific Reports volume 12, Article number: 20455

[21] "Graphene oxide (GO) is the oxidized form of graphene and has recently gained a lot of attention as a platform for tissue engineering applications." 2017

Nanofiber Composites for Biomedical ApplicationsMarc Burgelman et al., "SCAPS Manual Most Recent." 2019 UNIVERSITIET GENT

[22] M. Girish, B.M., Siddesh, H.S. and Satish, B.M. “Taguchi grey relational analysis for parametric optimization of severe plastic deformation process.” SN Appl. Sci. 1, 937 (2019). India: SpringerLink 2019.

[23] M. S. Baharudin, S. F. Abdullah, I. Ahmad, A. W. M. Zuhdi, A. H. Hasani, F. Za’abar, M. Malik and M. N. Harif, Jsc and Voc, “Optimization of Perovskite Solar Cell with Interface Defect Layer Using Taguchi Method.” 2018 IEEE International Conference on Semiconductor Electronics (ICSE). Selangor, Malaysia: IEEE 2018.

[24] S. Nair, S. B. Patel and J. V. Gohel, “Recent trends in efficiency-stability improvement in perovskite solar cells. Materials” Today Energy 17 (2020) 100449. Surat, India: Elsevier 2020.

[25] E. Widianto, Shobih, E. S. Rosa, K. Triyana, N. M. Nursam, and I. Santoso, “Performance analysis of carbon-based perovskite solar cells by graphene oxide as hole transport layer: Experimental and numerical simulation,” Opt. Mater. (Amst)., vol. 121, 2021, doi: 10.1016/j.optmat.2021.111584.

[26] M. Dadashbeika, D. Fathia, M. Eskandari, “Design and simulation of perovskite solar cells based on graphene and TiO2/graphene nanocomposite as electron transport layer.” 2020 Solar Energy 207 (2020) 917–924

[27] A Goje et al., "Design and Simulation of Lead-free Flexible Perovskite Solar Cell Using SCAPS-1D." 2023 IOP Conf. Ser.: Mater. Sci. Eng. 1278 012004

[28] Masood Mehrabian et al, "Simulating the thickness effect of the graphene oxide layer in CsPbBr3-based solar cells." 2021 Published by IOP Publishing Ltd Mater. Res. Express 8 (2021) 035509

[29] R. Pundir, G. H. V. C. Chary, and M. G. Dastidar, “Application of Taguchi method for optimizing the process parameters for the removal of copper and nickel by growing Aspergillus sp.,” Water Resour. Ind., vol. 20, pp. 83–92, 2018, doi: 10.1016/j.wri.2016.05.001

[30] T. Bao, “Graphene Oxide As an Oil Additive.” pp. 39230–39241, 2019.

[31] K. V. Sabarish, J. Baskar, and P. Paul, “Overview on L9 taguchi optimizational method,” Int. J. Adv. Res. Eng. Technol., vol. 10, no. 2, pp. 652–658, 2019, doi: 10.34218/IJARET.10.2.2019.062.

[32] J. H. Nkuissi Tchognia, B. Hartiti, A. Ridah, J. M. Ndjaka, and P. Thevenin, “Application of Taguchi approach to optimize the sol-gel process of the quaternary Cu2ZnSnS4 with good optical properties,” *Opt. Mater. (Amst).*, vol. 57, pp. 85–92, Jul. 2016, doi: 10.1016/J.OPTMAT.2016.04.023.